Conserved juxtamembrane domains in the yeast golgin Coy1 drive assembly of a megadalton-sized complex and mediate binding to tethering and SNARE proteins

Received for publication, February 20, 2019, and in revised form, April 26, 2019 Published, Papers in Press, May 9, 2019, DOI 10.1074/jbc.RA119.008107

Nadine S. Anderson and Charles Barlowe[1]

From the Department of Biochemistry and Cell Biology, Geisel School of Medicine at Dartmouth, Hanover, New Hampshire 03755

Edited by Phyllis I. Hanson

The architecture and organization of the Golgi complex depend on a family of coiled-coil proteins called golgins. Golgins are thought to form extended homodimers that are C-terminally anchored to Golgi membranes, whereas their N termini extend into the cytoplasm to initiate vesicle capture. Previously, we reported that the *Saccharomyces cerevisiae* golgin Coy1 contributes to intra-Golgi retrograde transport and binds to the conserved oligomeric Golgi (COG) complex and multiple retrograde Golgi Q-SNAREs (where SNARE is soluble NSF-attachment protein receptor). Here, using various engineered yeast strains, membrane protein extraction and fractionation methods, and *in vitro* binding assays, we mapped the Coy1 regions responsible for these activities. We also report that Coy1 assembles into a megadalton-size complex and that assembly of this complex depends on the most C-terminal coiled-coil and a conserved region between this coiled-coil and the transmembrane domain of Coy1. We found that this conserved region is necessary and sufficient for binding the SNARE protein Sed5 and the COG complex. Mutagenesis of conserved arginine residues within the C-terminal coiled-coil disrupted oligomerization, binding, and function of Coy1. Our findings indicate that the stable incorporation of Coy1 into a higher-order oligomer is required for its interactions and role in maintaining Golgi homeostasis. We propose that Coy1 assembles into a docking platform that directs COG-bound vesicles toward cognate SNAREs on the Golgi membrane.

The Golgi complex must accurately sort, process, and export secretory cargo while simultaneously maintaining its own composition to ensure continuous functionality (1, 2). Transport specificity is crucial for the Golgi complex to properly sort cargo while maintaining its own homeostasis, and this feat is achieved through a combination of dedicated trafficking factors, including small Rab GTPase networks (3), multisubunit tethering complexes (MTCs)[2] (4), soluble *N*-ethylmaleimide–sensitive factor attachment protein receptors (SNAREs) (5, 6), and a family of coiled-coil proteins called golgins (7–9). Each class of proteins is associated with executing distinct steps in vesicle transport at the Golgi: Rabs and golgins initiate vesicle capture (10), specific SNARE combinations drive vesicle fusion (11), and MTCs at the Golgi function somewhere in-between these stages (12–15). However, our understanding of how these components collaborate with one another to execute the capture and fusion of specific vesicles at the Golgi remains incomplete.

Golgins confer an initial layer of specificity to vesicle transport at the Golgi complex. These proteins are C-terminally anchored to Golgi membranes and are primarily composed of coiled-coils, suggesting the N termini of a golgin could extend hundreds of nanometers away from the Golgi membrane. Based on this topology, golgins have long been suspected of functioning as vesicle tethers (16). These predictions have largely been borne out: most mammalian golgins are sufficient to initiate vesicle capture *in vivo* (7), and the extreme N termini of these golgins are essential for these tethering events (17). Although ongoing work still seeks to define the vesicular signatures recognized by each golgin (18), our understanding of how vesicles are captured at the Golgi has advanced significantly.

Less is known about how a tethered vesicle traverses the distance from the N terminus of a golgin to the Golgi membrane. One model proposes that vesicles selectively diffuse toward the Golgi membrane through interactions with distinct Rab-binding sites distributed across the length of each golgin (19, 20). Golgin flexibility has also been implicated in delivering vesicles to Golgi membranes; for example, unstructured regions between the coiled-coils of GCC185 allow this protein's N terminus to come within 40 nm of its C terminus (21). Beyond how a vesicle approaches the Golgi membrane, it also remains unclear how vesicle capture is coordinated with recruitment of the requisite fusion factors.

Previously, we identified a role for the golgin Coy1 in intra-Golgi retrograde transport in *Saccharomyces cerevisiae*. Munro and co-workers (22) first characterized Coy1 and proposed a role for this golgin in Golgi transport based on genetic interactions with the SNAREs *GOS1* and *SEC22*. Subsequently, Warren and co-workers (23) reported that the mammalian homolog

This work was supported by National Institutes of Health Grant GM052549 and BioMT COBRE Grant P20 GM113132. The authors declare that they have no conflicts of interest with the contents of this article. The content is solely the responsibility of the authors and does not necessarily represent the official views of the National Institutes of Health.
This article was selected as one of our Editors' Picks.
This article contains Figs. S1–S3 and Table S1.

[1] To whom correspondence should be addressed. E-mail: charles.barlowe@dartmouth.edu.

[2] The abbreviations used are: MTC, multisubunit tethering complex; COG, conserved oligomeric Golgi complex; COPI, coat protein complex I; COPII, coat protein complex II; CBD, C-terminal binding domain; PMSF, phenylmethylsulfonyl fluoride; Ni-NTA, nickel-nitrilotriacetic acid; ANOVA, analysis of variance; ER, endoplasmic reticulum.

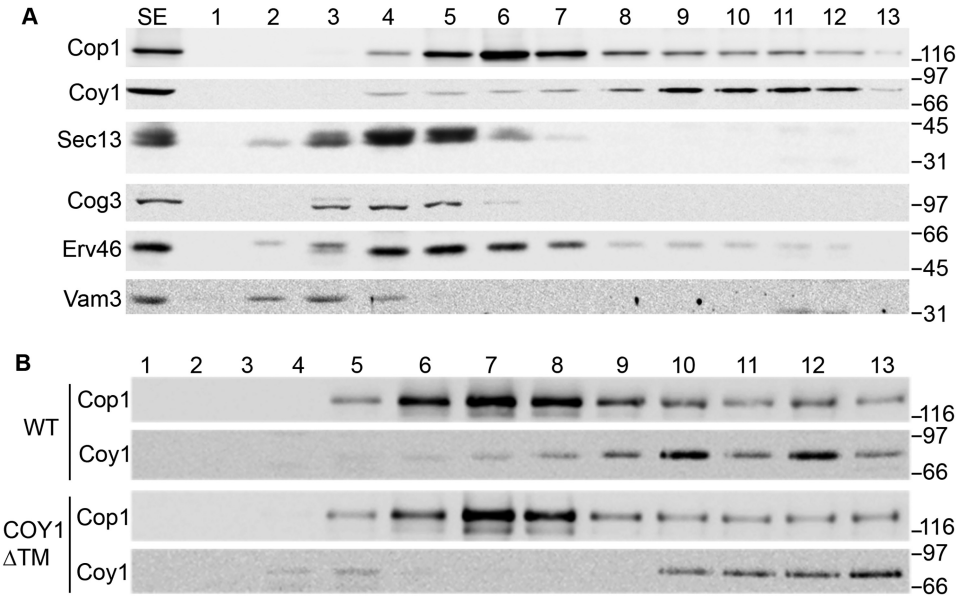

Figure 1. Coy1 sediments as a megadalton-sized complex on sucrose gradients. *A,* detergent-solubilized semi-intact cells derived from WT yeast (CBY740) were sedimented over a 5–45% sucrose gradient in an SW40 Ti rotor for 12 h at 4 °C. Samples were collected from the top to bottom of the gradient and resolved on 10.5% gels alongside a sample of the total soluble extract (*SE*). Immunoblotting was conducted with polyclonal antibodies against Coy1, Sec13, Cog3, Erv46, Vam3, and the α-subunit of coatomer, Cop1. *B,* integral membrane domain of Coy1 is not required for oligomerization. The experiment described in *A* was repeated to compare sedimentation of Coy1 from WT yeast cells (CBY740) and cells expressing Coy1ΔTM at the chromosomal locus (CBY3484). *Numbers at the right side* of this and all subsequent gels indicate the positions of a molecular mass marker in kDa.

of Coy1, CASP, specifically captured vesicles laden with recycled Golgi enzymes *in vitro*. However, Wong and Munro (7) later reported that CASP did not nucleate capture of any vesicle populations in their *in vivo* mitochondrial localization assay, calling into question this protein's capacity to function as a vesicle tether and its role in Golgi transport. We reported that cells lacking *COY1* display a defect in the retention of the cis-Golgi mannosyltransferase Och1 and that combining *coy1*Δ with other golgin mutations results in growth and glycosylation defects, consistent with a role for Coy1 in maintaining Golgi homeostasis. Coy1 physically interacts with all three Golgi retrograde Q-SNAREs and with the COG complex, an MTC required for retrograde transport on the Golgi (2, 6, 13, 24), suggesting a role for this golgin in vesicle docking and/or SNAREpin assembly.

To better understand Coy1's contribution to retrograde Golgi transport, we mapped the functionally essential regions of the protein. Here, we report that a conserved C-terminal region adjacent to Coy1's integral membrane domain is necessary and sufficient to bind both the SNARE Sed5 and the COG complex. Immediately N-terminal to this binding domain is a coiled-coil domain that is required for stable integration of Coy1 into a megadalton-sized complex. Mutation of conserved motifs within the minimal binding domain disrupts Coy1 interactions and *in vivo* function. These consequences are also observed when conserved arginine residues within the C-terminal coiled-coil domain are mutated. These arginine mutations also reduce the assembly of Coy1 into a larger complex, suggesting that the interactions and function of Coy1 depend on stable oligomerization. Based on these findings, we propose that Coy1 assembles into a docking platform that links COG-bound vesicles to a cognate set of fusogens on Golgi membranes.

Results

Previously, we reported that the golgin Coy1 elutes in the void volume of a Superose 6 gel-filtration column, which has an exclusion limit of 4 MDa (24). Two possibilities could explain this elution pattern: either Coy1 is incorporated into a large complex or it forms a smaller but highly extended assembly, as has been reported for other coiled-coil proteins of the Golgi complex (25). To distinguish between these possibilities, we sedimented detergent-solubilized membrane proteins from semi-intact cells through a 5–45% sucrose gradient. We monitored the distribution of Coy1 alongside other protein complexes of known size. The α-subunit of coatomer, Cop1, and a COPII coat subunit, Sec13, were detected in the middle and earlier sections of the gradient, consistent with their reported sedimentation coefficients of 13 S and 7.8 S, respectively (26–28). The integral membrane protein Erv46, which assembles into a complex of ~300 kDa (29), was also found in the middle of the gradient, whereas the syntaxin Vam3 was detected in the earliest fractions, consistent with a reported sedimentation coefficient of 4 S (30). Strikingly, Coy1 was most enriched at the bottom of the gradient. The Coy1-enriched fractions were well-resolved from the COG and COPI complexes, both of which interact transiently with Coy1 (Fig. 1*A*) (24, 31). The integral membrane domain of Coy1 did not contribute to this sedimentation pattern, as Coy1ΔTM was similarly enriched at the bottom of the gradient (Fig. 1*B*). In combination with our gel-filtration data (24), we conclude that the cytosolic domain of Coy1 assembles into a megadalton-sized complex.

To better understand how oligomerization of Coy1 affects its role in retrograde Golgi transport and interactions with the COG complex and SNAREs, we developed a mapping approach to identify the functionally essential regions of this protein.

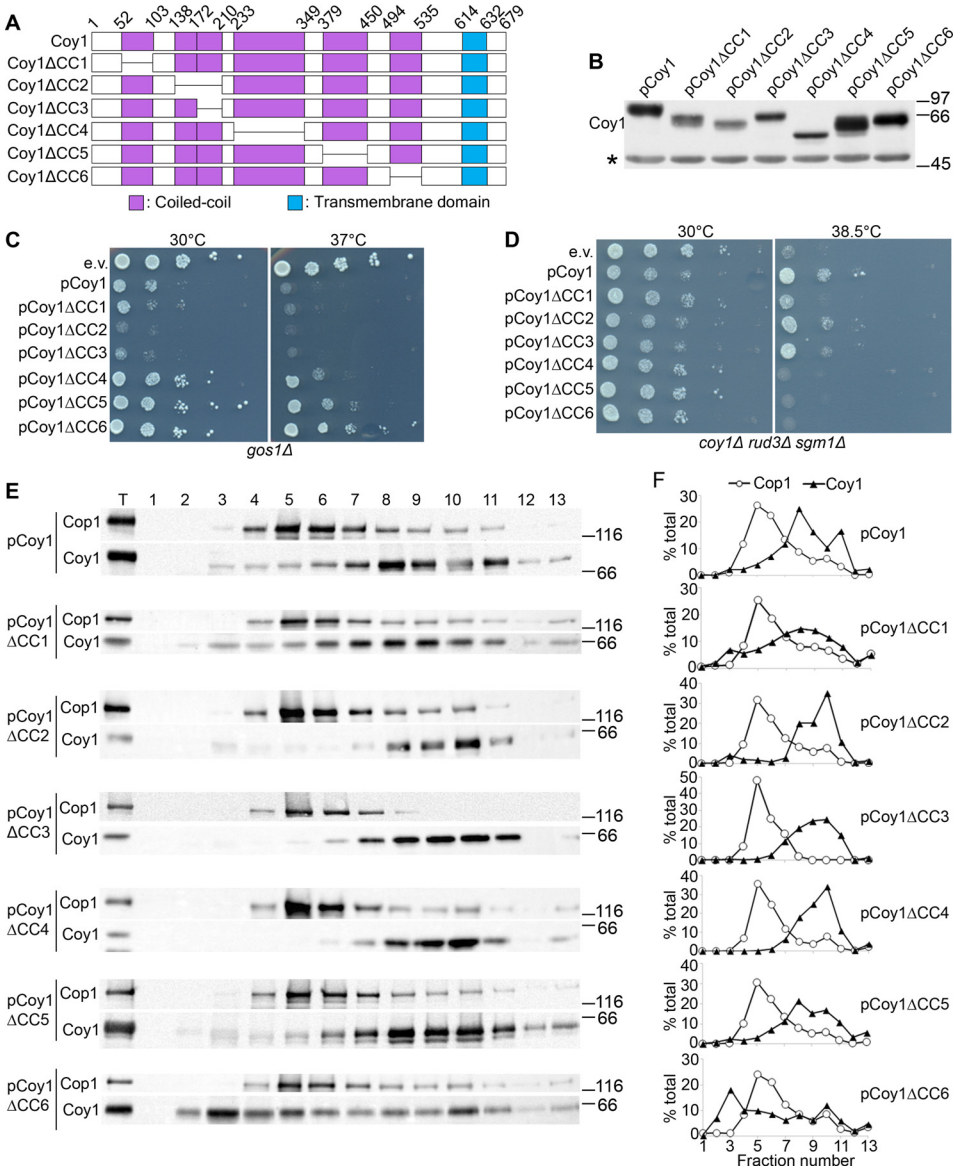

Figure 2. Functional analysis of the coiled-coil domains of Coy1. *A,* diagram of the constructs tested. Regions encoding Coy1's coiled-coil domains, including residues 52–103 (Coy1ΔCC1), 138–210 (Coy1ΔCC2), 172–210 (Coy1ΔCC3), 233–349 (Coy1ΔCC4), 379–450 (Coy1ΔCC5), and 494–535 (Coy1ΔCC6), were deleted from the *COY1* ORF on pRS426 vectors. *B,* expression of the Coy1ΔCC constructs. Semi-intact cells derived from the *coy1*Δ strain (CBY2660) carrying plasmid-borne Coy1 (pCoy1) or coiled-coil deletion constructs were analyzed on a 10.5% gel with Coy1 antiserum. The *asterisk* indicates an unknown species recognized by the antiserum that serves as a loading control. *C,* toxicity of *COY1* overexpression depends on its C-terminal coiled-coil domains. Serial dilutions prepared from the *gos1*Δ strain (CBY2679) carrying either an empty vector (*e.v.*) or the Coy1 constructs were spotted onto selective media and imaged after 72 h at the indicated temperatures. Overexpression of *COY1* induces a growth defect in this context, while cells bearing the ΔCC4, ΔCC5, or ΔCC6 truncations grow comparatively well. *D,* C-terminal coiled-coil domains of Coy1 are functionally essential. The *coy1*Δ *rud3*Δ *sgm1*Δ strain was transformed with plasmids as in *C* and cultured on selective media at either 30 °C or the restrictive temperature, 38.5 °C. Cells lacking a functional copy of Coy1 fail to grow at the restrictive temperature. *E,* C-terminal coiled-coil of Coy1 is required for oligomerization. Detergent-solubilized semi-intact *coy1*Δ cells (CBY2660) carrying the indicated plasmids were sedimented through sucrose gradients as described in Fig. 1. Fractions were analyzed on 10.5% gels and immunoblotted for Coy1 and Cop1. *Numbers* at the *top* of the gel denote fraction number and a sample of the total soluble extract. This image represents one of three independent experiments. *F,* quantification of *D,* based on densitometry using GeneSys software. Peak Coy1 levels are observed from fractions 8 to 10 in all instances except in the ΔCC6 truncation.

First, we examined the contribution of Coy1's predicted coiled-coil domains (32, 33) by individually deleting them from a 2-μm plasmid that expresses *COY1* under the strong constitutive *PHO5* promoter (Fig. 2*A*). After verifying expression of these constructs (Fig. 2*B*), we tested their ability to induce a growth defect in the *gos1*Δ strain. As reported previously (22), overexpression of *COY1* induced a strong growth defect in *gos1*Δ cells. This growth defect was still apparent in cells overexpressing Coy1 ΔCC1, ΔCC2, or ΔCC3, but it was ameliorated in cells bearing the ΔCC4, ΔCC5, and ΔCC6 constructs (Fig. 2*C*). At elevated temperatures, a graded phenotype was apparent, with truncations closer to the C terminus of Coy1 eliciting a less severe phenotype than those near the N terminus. These results reveal that the middle and C-terminal coiled-coils are required for Coy1 toxicity in *gos1*Δ cells.

In a reciprocal approach, we examined whether these constructs could rescue the *coy1*Δ *rud3*Δ *sgm1*Δ strain, which cannot grow at high temperatures without plasmid-borne *COY1*

(24). Each transformant grew at a similar rate at lower temperatures, whereas cells bearing an empty vector were inviable at the restrictive temperature. Growth was rescued by the WT, ΔCC2, and ΔCC3 constructs. Some growth was apparent in cells carrying the Coy1ΔCC1 plasmid, but not to the same level as the former constructs, suggesting Coy1 function had been partially compromised. Cells bearing the ΔCC4, ΔCC5, and ΔCC6 plasmids were completely inviable (Fig. 2*D*). Thus, both the toxicity and rescue assays pinpointed these coiled-coils as essential for Coy1 function.

To analyze the contribution of these coiled-coils to oligomerization of Coy1, we resolved solubilized yeast membranes expressing these constructs as their sole copy of Coy1 on sucrose gradients. Notably, although these constructs were all highly overexpressed, the sedimentation pattern of plasmid-borne Coy1 remained comparable with that of the endogenously expressed protein (Fig. 2*E*). Smaller assemblies of Coy1 do not accumulate upon overexpression, which suggests that Coy1 assembles into a megadalton-sized complex on its own. Five of the six Coy1ΔCC constructs exhibited a similar sedimentation pattern, with a majority of each protein peaking after Cop1 (Fig. 2*F*). In contrast, Coy1ΔCC6 exhibited a broad distribution with one peak at the top of the gradient and a second minor peak at the same position as WT Coy1 (Fig. 2, *E* and *F*), suggesting that formation of this complex was strongly reduced but not abolished. This result indicates that the C-terminal coiled-coil of Coy1 is required for the stable incorporation of this protein into a higher-order oligomer.

We next analyzed whether these coiled-coil truncations affected binding of Coy1 to either Sed5 or the COG complex in bead-based pulldown assays. However, we were unable to identify a single coiled-coil domain that, when deleted, abolished these interactions.[3] We instead tested whether truncation of the three functionally nonessential N-terminal coiled-coils (amino acids 1–210) or the entire coiled-coil region (1–535) affected these interactions (Fig. 3*A*). WT Coy1 was specifically recovered with GST–Sed5 and lobe A of the COG complex, which consists of Cog1, Cog2, Cog3, and Cog4 (24, 34). However, these interactions were not as robust as observed previously (24). This difference is likely attributable to the inclusion of the transmembrane domain in these N-terminal truncations, suggesting that Coy1's integral membrane domain may limit these interactions or that some binding activity is lost following detergent solubilization. The first truncation, spanning residues 211–679, bound to Sed5 and COG to a similar extent as the full-length protein. Surprisingly, specific interactions with Sed5 and COG were not only preserved in the 536–679 truncation, these interactions appeared far more robust than in the other constructs (Fig. 3, *B* and *D*). Relative to WT Coy1, recovery of this C-terminal fragment was on average nearly three times higher with Sed5 and 15-fold higher with COG (Fig. 3, *C* and *E*). These interactions were abolished when Coy1 was C-terminally truncated at residue 535 (Fig. 3, *F–I*), indicating that Coy1(536–679) is both necessary and sufficient to interact with Sed5 and the COG complex.

[3] N. S. Anderson and C. Barlowe, unpublished observations.

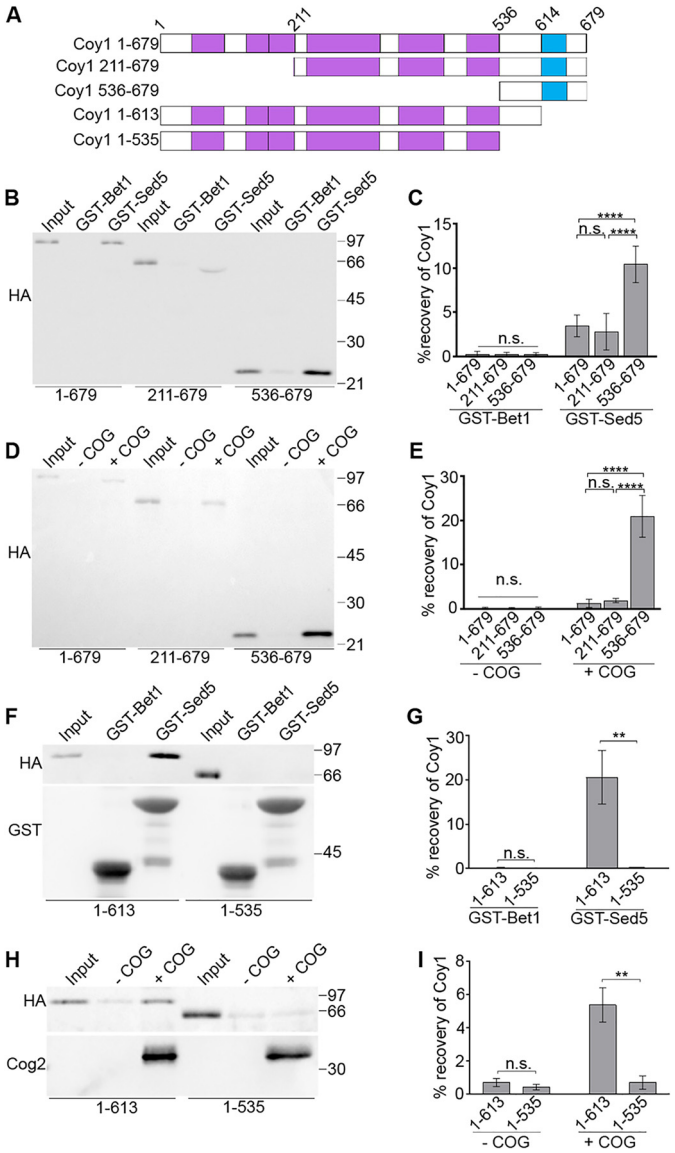

Figure 3. C terminus of Coy1 is necessary and sufficient to bind the COG complex and Sed5 *in vitro*. *A,* diagram of constructs used in this study. *B,* C terminus of Coy1 is sufficient to selectively bind GST–Sed5. Recombinant Sed5 and Bet1 were immobilized on GSH-agarose resin and incubated with solubilized membrane extracts from *pGAL-COY1*(1–679)*-3xHA* (CBY3484), *pGAL-COY1*(*211–679*)*-3xHA* (CBY5544), and *pGAL-COY1*(*536–679*)*-3xHA* (CBY5545) as described under "Experimental procedures." After washing the resin, bound proteins were eluted with sample buffer. 1% of the reaction inputs and 20% of the eluates were resolved on 11.5% SDS-polyacrylamide gels and immunoblotted for HA. *C,* truncation of coiled-coil domains increases binding to Sed5. Mean recovery of the indicated Coy1 constructs with either Bet1 or Sed5 was calculated from six independent experiments. *D,* C terminus of Coy1 is sufficient to selectively bind the COG complex. Binding assays with recombinant COG complex on Ni-NTA resin and solubilized membranes were conducted as in *B*. Background binding was monitored by incubating solubilized membranes with untreated resin (−*COG lanes*). *E,* truncation of coiled-coil domains improves binding of Coy1 to the COG complex. Mean recovery of Coy1 with Ni-NTA resin without (−) or with (+) recombinant COG complex was quantified from six independent experiments described in *D*. *F,* C terminus is essential for Coy1 to bind Sed5. SNARE-binding assays using cytosols from *coy1*Δ semi-intact cells (CBY2660) expressing the indicated plasmid-borne Coy1 constructs were performed as in *B*. *G,* mean recovery of Coy1 constructs from three independent experiments described in *F*. *H,* C terminus of Coy1 is essential for COG complex binding. Binding to COG was performed as described in *D* using cytosol as in *F*. *I,* mean recovery of Coy1 with or without COG, quantified from three independent experiments described in *H*. In all panels of this figure, *error bars* indicate standard deviation, and statistical analyses were performed with two-way ANOVA followed by Tukey's test, with *n.s.*, not significant; **, $p < 0.005$; ****, $p < 0.0001$.

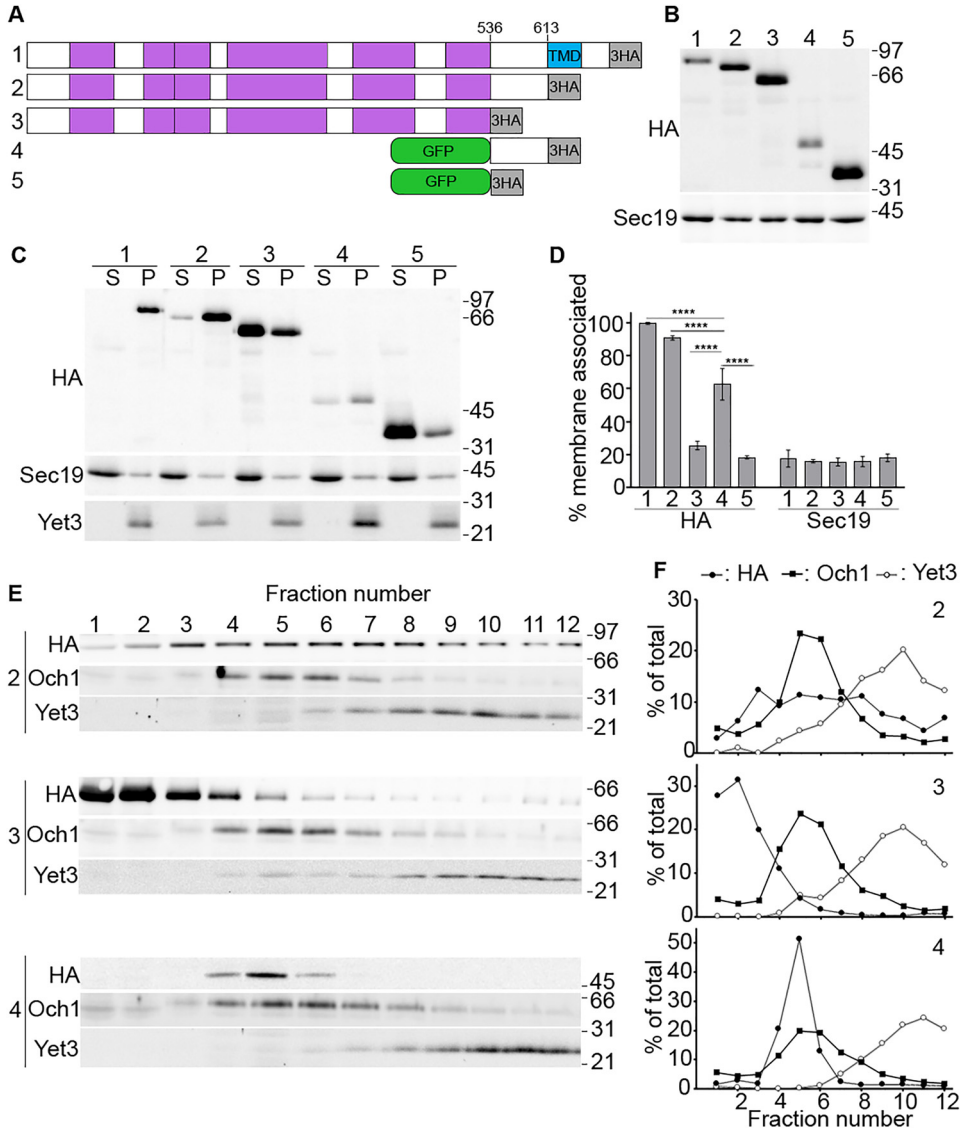

Figure 4. C-terminal domain of Coy1 confers Golgi membrane targeting information. *A,* diagram of constructs used in the experiments described in this figure and Fig. 5. *B,* comparison of expression levels. Samples of semi-intact *coy1*Δ cells expressing the indicated constructs under the constitutive *TPI* promoter were resolved on 11.5% gels and immunoblotted with anti-HA and anti-Sec19 (loading control). *C,* C-terminal domain of Coy1 confers membrane targeting information. Semi-intact cells expressing the indicated constructs were resuspended in buffer and centrifuged at 54,000 rpm as described under "Experimental procedures." Equivalent amounts of the soluble (*S*) and membrane-pellet (*P*) fractions were resolved on 11.5% SDS-polyacrylamide gels and immunoblotted for HA, Sec19, and Yet3. *D,* quantification of average membrane association of the HA-tagged constructs and, as a control, Sec19 from five independent experiments as described in *C*. *Error bars* indicate standard deviation, and statistical analyses were performed with two-way ANOVA followed by Dunnett's test with ****, $p < 0.0001$. *E,* C-terminal domain of Coy1 is necessary and sufficient for Golgi membrane targeting. Membranes from *coy1*Δ cells expressing the indicated constructs were separated over 18–60% sucrose gradients. Fractions were collected from the top of gradients and resolved on 11.5% gels for immunoblotting against the HA epitope and the integral Golgi (Och1) and ER (Yet3) membrane proteins. The blots depicted represent one of three independent experiments. *F,* densitometric quantification of blots displayed in *E*, showing distribution of Coy1-HA, Och1, and Yet3. The majority of Coy1(1–613) cofractionates with the Golgi marker Och1. Coy1(1–535) stays at the top of the gradient, and GFP-Coy1(536–613) is enriched in the Golgi fractions.

To complement these *in vitro* binding assays, we tested whether the cytosolic portion of Coy1's C-terminal binding domain (CBD) localized to Golgi membranes. We constructed plasmids encoding this domain sandwiched between an N-terminal superfolder GFP variant (35) and a C-terminal 3xHA tag with the intent of visualizing its localization *in vivo* (Fig. 4*A*). However, we were unable to detect expression of this fusion protein when encoded on a centromeric plasmid. Overexpression of this construct from a 2-μm vector yielded a detectable signal, although the abundance of this fusion protein was reduced relative to the other Coy1 truncations (Fig. 4*B*). We elected to examine the distribution of this fusion protein through bulk fractionation assays instead of live-cell imaging.

We first asked whether the CBD was important for Coy1ΔTM to remain membrane-associated. Membranes derived from *coy1*Δ cells carrying plasmids encoding various Coy1 truncations or GFP were centrifuged at a high speed to generate a cytosol-enriched supernatant and a membrane pellet fraction. The integral membrane protein Yet3 was exclusively detected in the membrane pellet fractions, whereas Sec19, the yeast homolog of GDP-dissociation inhibitor, remained largely enriched in the supernatant fraction in each

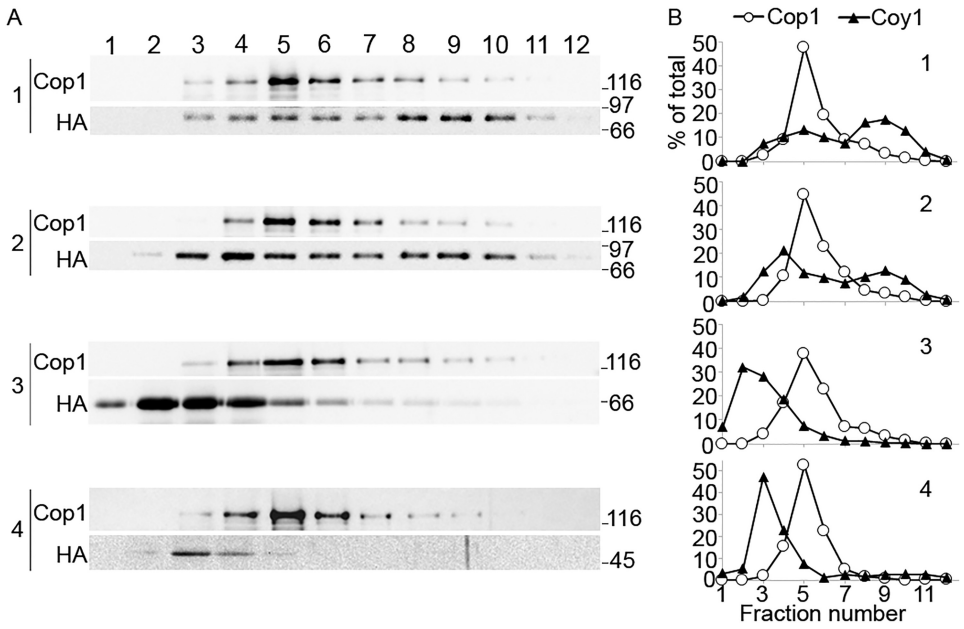

Figure 5. C-terminal binding domain is necessary but not sufficient for oligomerization of Coy1. *A,* detergent-solubilized extract from *coy1*Δ cells expressing the constructs described in Fig. 4*A* were sedimented over sucrose gradients, and fractions were collected and analyzed by immunoblotting as in Fig. 1. This blot represents one of four distinct experiments. *B,* densitometric quantification of the HA and Cop1 signals from *A*. The 1–535 and GFP(536–613) constructs are only detected at the top of the gradient.

assay (36, 37). As expected, GFP was largely detected in the cytosolic fraction, although ~18% could be detected in the pellet, reflecting some carryover with membrane proteins. Full-length Coy1 was also exclusively detected in the pellet, whereas 91% of Coy1ΔTM was also found in the membrane fraction, as reported previously (24). In contrast, the Coy1(1–535) construct that lacks the CBD exhibited a primarily cytosolic distribution, with only 26% remaining in the membrane pellet (Fig. 4, *C* and *D*). Despite low levels of expression (Fig. 4*B*), over 60% of the GFP–CBD construct was detected in the membrane pellet (Fig. 4, *C* and *D*). This construct was not as strongly associated with membranes as Coy1ΔTM, suggesting that other cytosolic regions of Coy1 may stabilize interactions with membranes. Regardless, these data support a role for Coy1's C-terminal domain in engaging with other membrane-associated factors.

Next, we examined whether the CBD specifically associated with Golgi membranes by resolving organelles from lysed semi-intact *coy1*Δ cells expressing the cytosolic Coy1 constructs on sucrose gradients. In each experiment, Golgi membranes marked by Och1 were enriched in the middle of the gradient, whereas denser ER membranes marked by Yet3 pelleted at the bottom of the tube. Although Coy1ΔTM exhibited a broad sedimentation profile, most of this protein co-fractionated with Golgi membranes, as reported previously (24). In contrast, Coy1(1–535) fractionated at the top of the gradient, reflecting its cytosolic localization. Strikingly, GFP–CBD was consistently enriched in the Golgi membrane fractions (Fig. 4, *E* and *F*). The strong association of this construct with Golgi membrane fractions provides further support for the CBD in interacting with other Golgi-associated proteins, including but not limited to Sed5 and the COG complex.

To analyze the contribution of the CBD to Coy1 oligomerization, *coy1*Δ cells expressing these same plasmids were detergent-solubilized, and protein complexes were resolved on sucrose gradients. As observed previously, full-length Coy1 was enriched in the bottom of the gradient (Fig. 5). Coy1ΔTM also sediments as a large oligomer, although it exhibits a split distribution between the top and bottom of the gradient (Fig. 5*B*). This result contrasts with the sedimentation pattern observed when Coy1ΔTM is expressed from its endogenous locus (Fig. 1*B*), suggesting that the integral membrane domain stabilizes oligomerization when Coy1 levels are very high. Both the Coy1(1–535) and GFP–CBD constructs were solely detected in the earliest fractions of the gradient, indicating that the CBD is necessary but not sufficient for oligomerization of Coy1 (Fig. 5).

To analyze the functional relevance of the CBD, we first tested whether this region could induce a growth defect in *gos1*Δ. We constructed a series of Coy1 constructs in which Coy1 was N-terminally truncated either after the dispensable N-terminal coiled-coils (encompassing residues 233–679), or the first (379–679), second (494–679), or third (536–679) essential coiled-coils. Expression of full-length Coy1 and the first truncated construct (233–679) caused a strong growth defect in *gos1*Δ, consistent with this N-terminal region being dispensable for Coy1 toxicity. Cells expressing the 379–679 construct grew slightly less robustly than those carrying an empty vector. Notably, expression of the 494–679 construct resulted in a more severe growth defect than the preceding truncation, suggesting that residues 379–493 limit the toxicity of Coy1. Cells expressing the membrane-anchored CBD(536–679) phenocopied the empty vector control (Fig. S1). These results indicate that full Coy1 activity requires its three most C-terminal coiled-coils, but partial activity is still apparent until the most C-terminal coiled-coil of Coy1 is truncated.

The C terminus of Coy1 belongs to a conserved protein family termed the CASP C-terminal region (Pfam entry: PF08172) (38). Alignment of this family using the program Jalview revealed a series of highly conserved residues within the last

coiled-coil domain and the CBD of Coy1 (39). We asked whether these conserved residues were important for Coy1 functionality. We built a series of *COY1* constructs on a pRS416 *pGAL1* backbone in which either the ^{496}QRDRFRXR^{503}, ^{536}YERIRY^{541}, or ^{604}KX_5KXXR^{613} motifs were mutagenized to alanines, with *X* denoting residues that were not mutagenized (Fig. 6*A*). Each of these constructs was highly overexpressed relative to endogenous Coy1 (Fig. S2). Overexpression of WT

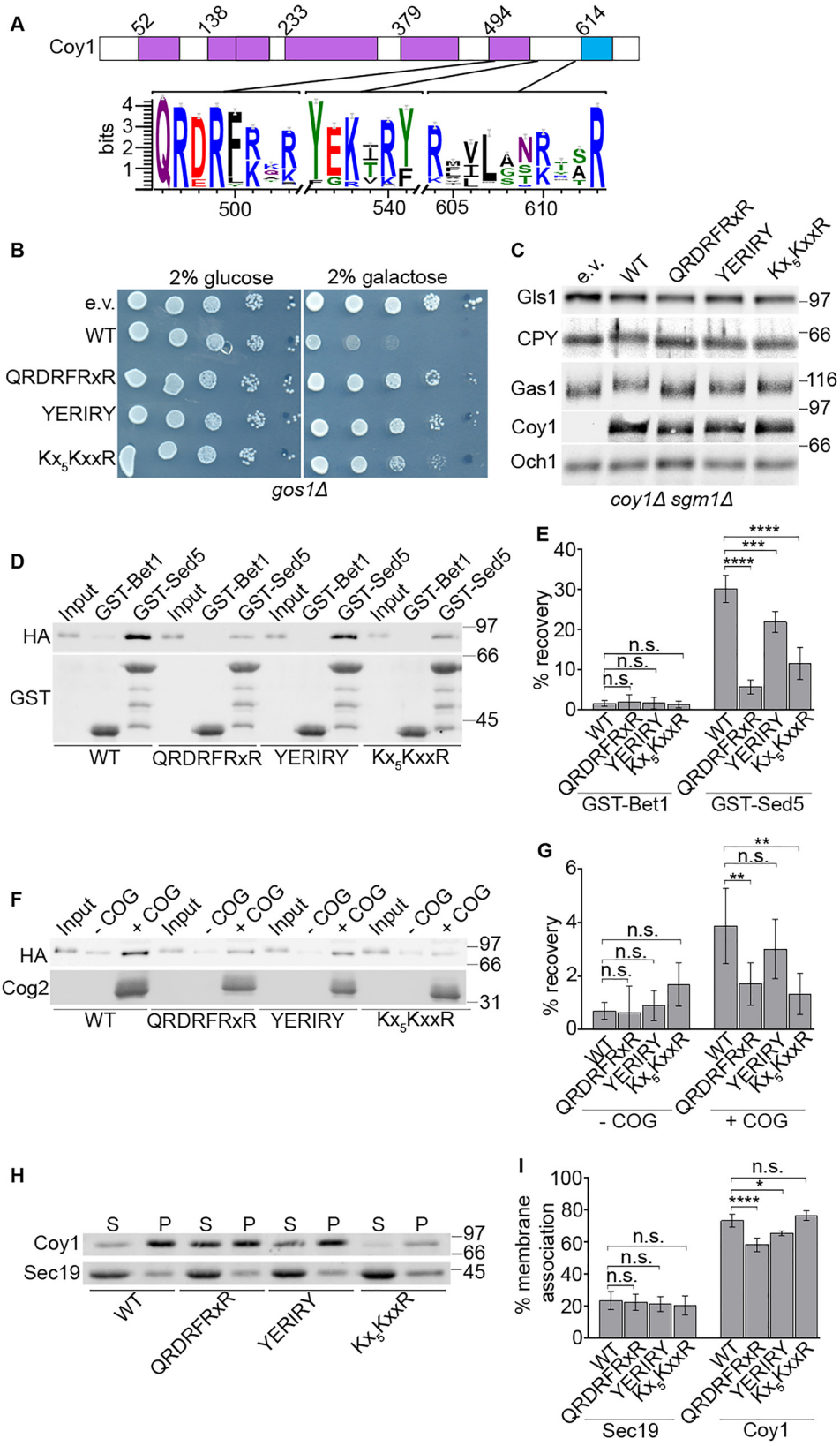

Coy1 induced a strong growth defect in *gos1*Δ as expected, but cells expressing the mutant Coy1 variants all grew comparatively well. The Coy1 KX_5K*XXR* construct induced an intermediate phenotype, yielding cells that grew more robustly than those expressing WT Coy1, but not as well as those carrying either an empty vector or the other two Coy1 motif mutations (Fig. 6*B*). In a reciprocal experiment, we examined whether these constructs could complement the glycosylation defects observed in the *coy1*Δ *sgm1*Δ strain rather than the temperature sensitivity of the *coy1*Δ *sgm1*Δ *rud3*Δ strain. The apparent molecular weights of two secretory glycoproteins, Gas1 and CPY, are reduced in *coy1*Δ *sgm1*Δ, and this defect can be corrected by supplying *COY1* on a plasmid (24). However, a plasmid encoding the QRDRFR*X*R Coy1 construct failed to rescue Gas1 and CPY glycosylation, whereas expression of the YERIRY and KX_5K*XXR* constructs resulted in an intermediate phenotype (Fig. 6*C*). We conclude that the conserved motifs in Coy1's C-terminal coiled-coil and binding domain are required for optimal Coy1 function in Golgi transport.

We next analyzed whether these motif mutations affected Coy1's ability to bind Sed5 or the COG complex. Each Coy1 variant was recovered with GST–Sed5 and not with GST–Bet1, but recovery of the mutant proteins was reduced relative to WT Coy1ΔTM. Notably, recovery of Coy1 with Sed5 was more severely impaired in the presence of the QRDRFR*X*R and KX_5K*XXR* mutations than with the YERIRY mutation (Fig. 6, *D* and *E*). A similar pattern was observed when binding to COG was monitored: the QRDRFR*X*R and KX_5K*XXR* mutations reduced recovery of Coy1ΔTM, whereas the YERIRY mutation did not significantly affect binding (Fig. 6, *F* and *G*). Thus, the conserved QRDRFR*X*R and KX_5K*XXR* motifs are essential for Coy1's ability to efficiently bind Sed5 and the COG complex.

Membrane association of Coy1ΔTM constructs was also monitored as an alternative means of analyzing the impact of the indicated mutations on Coy1's protein–protein interactions. As expected, Coy1ΔTM remains enriched in the membrane fraction, whereas the QRDRFR*X*R and YERIRY mutations result in a shift to the cytosolic fraction (Fig. 6, *H* and *I*). Although these mutations disrupt membrane association of Coy1ΔTM, they do not do so as drastically as truncation of the entire C-terminal binding domain (Fig. 4, *C* and *D*). This result suggests that some of Coy1's interactions with membrane-associated proteins are preserved when these mutations are present. The KX_5K*XXR* mutation did not appreciably disrupt membrane association of Coy1ΔTM (Fig. 6, *H* and *I*). However, protein levels of the Coy1ΔTM KX_5K*XXR* construct were reduced by nearly 85% relative to the other constructs, suggesting that this mutation may destabilize the protein and result in its degradation. This instability appeared to arise from the combination of the KX_5K*XXR* and ΔTM mutations, as the full-length Coy1 KX_5K*XXR* protein is expressed at levels comparable with the WT protein and the other mutants (Fig. S2).

We next tested whether these mutations affected Coy1's capacity to oligomerize by monitoring sedimentation of solubilized membranes from *coy1*Δ cells that expressed full-length Coy1 on a centromeric plasmid under the *TPI* promoter. As a control, we also monitored sedimentation of Cop1, which peaked in the same fractions in each experiment. WT Coy1 was enriched in the bottom of the sucrose gradient, as were the YERIRY and KX_5K*XXR* mutants, indicating that these residues are not involved in Coy1 oligomerization. The QRDRFR*X*R mutation resulted in a shift of Coy1 to the first fractions of the gradients, along with a minor secondary peak at the bottom of the gradient (Fig. S3), similar to the sedimentation pattern observed when the entire C-terminal coiled-coil of Coy1 (ΔCC6) is truncated (Fig. 2, *E* and *F*). We conclude that the conserved QRDRFR*X*R motif is essential for stable oligomerization of Coy1.

Finally, we examined whether single point mutations within the QRDRFR*X*R motif could disrupt Coy1's function, oligomerization, and interactions. We focused on residues predicted to lie within the hydrophobic core of this coiled-coil domain, as these residues often determine a coiled-coil's oligomeric state (40, 41). Within this motif, Phe-500 and either Arg-497 or Arg-503, depending on the register, were mapped by the coiled-coil prediction software Waggawagga to the hydrophobic core of the C-terminal coiled-coil domain (Fig. 7*A*) (42). As bulky and charged residues are infrequently found in this hydrophobic position, we asked whether converting these residues to the more commonly observed leucine affected Coy1's function (43). Growth of the *gos1*Δ strain was still inhibited by overexpression of *COY1 F500L*, whereas cells expressing the R497L or R503L mutation grew as well as those carrying the full QRDRFR*X*R mutated construct (Fig. 7*B*). Moreover, the R497L

Figure 6. Conserved motifs within the C-terminal domain of Coy1 are essential for Coy1 function and interactions. *A,* WebLogos of conserved regions within the C terminus of Coy1 assembled from an alignment of the 635 CASP_C sequences accessible on pFAM (PF08172). The *left panel* represents residues 496–503 and maps to the last coiled-coil of Coy1, and the *middle* and *right panels* correspond to residues 536–541 and 604–613, both of which are present in the CBD. *B,* alanine swapping of conserved motifs in Coy1's C-terminal coiled-coil and binding domain abolish toxicity of *COY1* overexpression. Serial dilutions on media with either glucose or galactose were prepared from log-phase cultures of *gos1*Δ cells (CBY2679) carrying an empty vector (*e.v.*) or centromeric plasmids encoding *pGAL1-COY1* constructs in which indicated residues were mutagenized to alanines. Cultures were grown at 30 °C. Expression of WT *COY1* produces a strong growth defect, whereas the motif mutations cause a milder phenotype. *C,* conserved motifs in Coy1 required for normal Golgi glycosylation activity. Cultures of *coy1*Δ *sgm1*Δ cells carrying either an empty vector (*e.v.*) or the indicated *COY1* constructs were resolved on 8% polyacrylamide gels and blotted for Gls1 and Och1 as loading controls, Coy1, and the secretory glycoproteins CPY and Gas1. Note that under-glycosylation of CPY and Gas1 in the *coy1*Δ *sgm1*Δ strain is fully corrected by WT Coy1 but not the mutated Coy1 proteins. *D,* cytosols from *coy1*Δ cells (CBY2660) carrying the indicated *pGAL1-Coy1ΔTM* constructs were prepared and used in SNARE-binding assays as described in Fig. 3*F*. *E,* quantification of mean percent recovery of Coy1ΔTM proteins with the indicated SNAREs from four independent experiments described in *C*. *F,* conserved motifs in Coy1 are essential for binding COG. Cytosols containing indicated Coy1ΔTM proteins were prepared as in *D* and monitored in binding assays with immobilized COG complex as described in Fig. 3*H*. *G,* quantification of mean recovery of Coy1ΔTM proteins with Ni-NTA resin incubated with (+) or without (−) COG complex from eight independent experiments. *Error bars* denote standard deviation. *H,* mutation of conserved residues within the C terminus of Coy1 disrupts membrane association of Coy1ΔTM. Membrane association of the indicated Coy1ΔTM constructs, expressed in *coy1*Δ (CBY2660) under the *TPI* promoter, was monitored as described in Fig. 4, *C* and *D*. WT Coy1ΔTM remains enriched in the membrane pellet, whereas constructs with the QRDRFR*X*R and YERIRY mutations partially shift to the supernatant fraction. *I,* quantification of average membrane association of Sec19 and Coy1 from six independent experiments described in *G*. In the relevant panels, *error bars* all denote standard deviation and statistical analyses were performed by two-way ANOVA followed by Dunnett's test, with *n.s.*, not significant; *, $p < 0.05$; **, $p < 0.005$; ***, $p < 0.001$; ****, $p < 0.0001$.

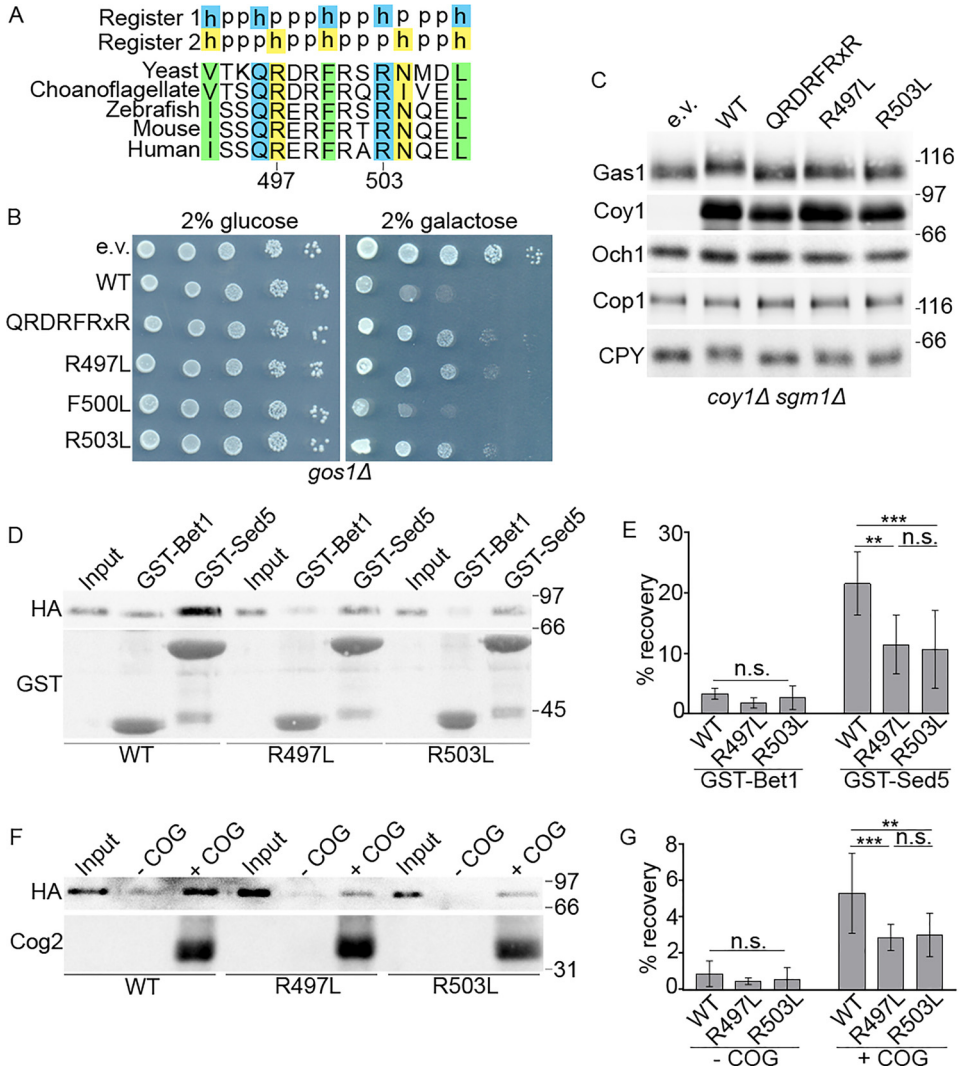

Figure 7. Interactions and oligomerization of Coy1 depend on conserved arginine residues within the C-terminal coiled-coil. *A,* alignment of the coiled-coil sequences surrounding the QRDRFR*X*R motif from various eukaryotes. The predicted heptad repeat registers with the hydrophobic positions highlighted are depicted above. Conserved arginine residues at positions 497 or 503 are predicted to map to the hydrophobic core. *B,* R497L and R503L mutations disrupt Coy1 toxicity. Growth rate assays of *gos1*Δ cells carrying either an empty vector (*e.v.*) or plasmids encoding Coy1 constructs under the *GAL1* promoter were set up at 30 °C on minimal media with either glucose or galactose as the sole carbon source. Expression of WT Coy1 induces a growth defect that is ameliorated by the QRDRFR*X*R motif mutation. This growth defect is also attenuated by the R497L and R503L point mutations, and it persists in the presence of the F500L mutation. *C,* R497L and R503L point mutations disrupt the function of Coy1 in Golgi transport. Lysates from *coy1*Δ *sgm1*Δ cells expressing either an empty vector or plasmids indicated the Coy1 constructs were resolved over 8% gels and blotted against Gas1, Coy1, and CPY. Och1 and Cop1 were monitored as loading controls. *D,* R497L and R503L mutations weaken the interaction between Coy1 and Sed5. SNARE-binding assays using cytosol from *coy1*Δ cells expressing the indicated Coy1ΔTM constructs was conducted as described in Fig. 3*F*. *E,* quantification of Coy1 recovery from *D* ($n = 5$). *Error bars* indicate standard deviation. Statistical analyses were performed with two-way ANOVA followed by Tukey's test with *n.s.*, not significant; ***, $p < 0.001$ and **, $p < 0.005$. *F,* binding of COG by Coy1 depends on Arg-497 and Arg-503. *In vitro* COG-binding assays using cytosol from *coy1*Δ cells expressing the indicated *Coy1ΔTM* constructs were conducted as described in Fig. 3*H*. *G,* quantification of Coy1 recovery from *F* ($n = 7$). Statistical tests were performed as described in *E*.

and R503L Coy1 constructs failed to completely restore glycosylation of Gas1 and CPY in *coy1*Δ *sgm1*Δ, indicating that these point mutations partially disrupt Coy1's function (Fig. 7*C*). Like the QRDRFR*X*R mutation (Fig. 6, *D–G*), the R497L and R503L mutations reduced the binding of Coy1ΔTM to both Sed5 (Fig. 7, *D* and *E*) and the COG complex (Fig. 7, *F* and *G*). Finally, the R497L and R503L mutations shifted Coy1's sedimentation pattern toward the top of the gradient (Fig. 8) in a similar manner as the motif mutation and C-terminal coiled-coil deletion (Fig. 2, *E* and *F*, and Fig. S3). These results indicate that Arg-497 and Arg-503 are required for stable oligomerization of Coy1 and suggest that the assembly of Coy1 into a higher-order structure is essential for its interactions and *in vivo* function.

Discussion

Transport specificity underlies compartmentation of the Golgi complex and depends on the activity of golgins, SNAREs, and MTCs, among other factors (4, 10, 15). A coherent understanding of how these components interface together to execute vesicle capture and fusion at the Golgi remains lacking. The work described here supports a model in which the golgin Coy1 assembles into a docking platform that directs tethering factors toward the requisite fusion machinery to maintain Golgi homeostasis.

Golgins are often depicted as rod-shaped homodimers (16). Our gel-filtration and sucrose-gradient sedimentation assays of

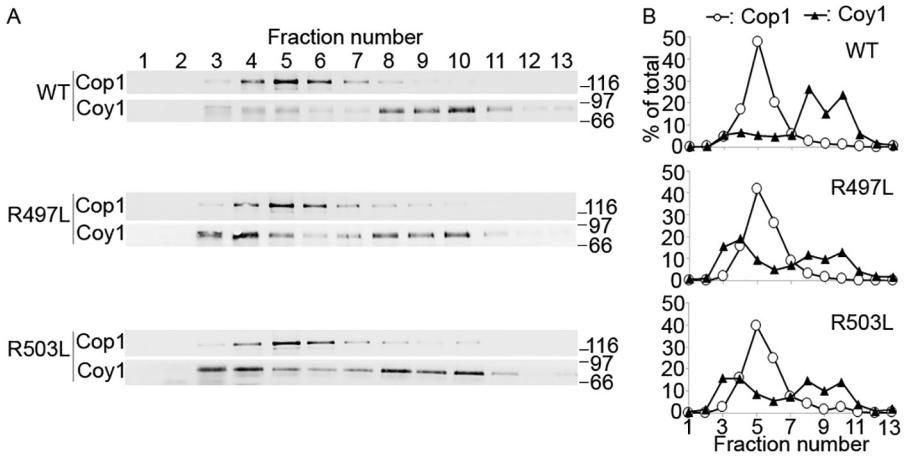

Figure 8. R497L and R503L point mutations disrupt oligomerization of Coy1. *A,* sucrose-gradient sedimentation assays using detergent-solubilized membrane extracts from *coy1*Δ cells expressing the indicated Coy1 constructs were conducted as described in Fig. 1. This blot represents one of three independent experiments. *B,* quantification of immunoblot signal from *A*. Cop1 (*open circles*) peaks at fraction 5 in each experiment. Coy1 (*black triangles*) sediments between fractions 8 and 10, but the R497L and R503L point mutations partially shift Coy1 toward the top of the gradient.

yeast membrane extracts indicate that Coy1 is instead incorporated into a much larger complex (24). This sedimentation pattern cannot be attributed to aggregation induced by the integral membrane domain of Coy1, as endogenously-expressed Coy1ΔTM sediments at a similar position as full-length Coy1. Furthermore, the observation that Coy1 sediments at one or two discrete positions suggests that this protein is not indiscriminately forming oligomers but is instead forming a complex of a defined size (Fig. 1, *A* and *B*). Determining the exact oligomeric state of Coy1 will require subjecting the purified, active complex to more precise techniques such as analytical ultracentrifugation or native MS (44–46).

Notably, overexpression of full-length Coy1 from either a multicopy plasmid (Fig. 2*A*) or by the strong *GAL1* promoter does not result in an accumulation of unassembled Coy1 in either sucrose-gradient or gel-filtration assays, respectively (24). If Coy1 was present in a heteromeric complex, its overexpression would be expected to saturate the availability of other binding partners and lead to an accumulation of unassembled Coy1. This result has not been observed, suggesting that Coy1 assembles into the core of this complex on its own. However, this does not exclude the possibility that other subunits decorate this complex.

Golgins are thought to act in vesicle transport by N-terminally capturing incoming vesicles. In contrast, our genetic toxicity and complementation assays have highlighted the importance of the C-terminal half of Coy1. Truncation of any of the putative coiled-coil domains between residues 233 and 535 diminished Coy1's capacity to induce a growth defect in the *gos1*Δ strain, whereas the same constructs also failed to rescue viability of the *coy1*Δ *rud3*Δ *sgm1*Δ strain at a restrictive temperature (Fig. 2, *C* and *D*). Notably, *gos1*Δ cells overexpressing a Coy1 truncation that lacks its N-terminal 232 residues exhibit a growth defect that is as robust as cells expressing full-length Coy1 (Fig. S1). The dispensability of Coy1's N terminus in these assays does not explicitly exclude a function for this region in membrane trafficking or other processes. However, the essentiality of the middle and C-terminal regions suggests a more membrane-proximal role for Coy1 than other golgin proteins.

We have identified two discrete regions of Coy1 that mediate different protein–protein interactions. One region spanning 78 residues between Coy1's C-terminal coiled-coil and its transmembrane domain is both necessary and sufficient for Coy1's interactions with the SNARE Sed5 and the COG complex, a region we have termed the C-terminal binding domain (Fig. 3). Complementing these *in vitro* binding experiments, membrane fractionation assays revealed a tight association between the CBD and Golgi membranes (Fig. 4). The strength of this association raises the possibility that the CBD interacts with other unidentified Golgi-associated factors. This inference is lent further support by the observation that the motif mutations that disrupted binding to Sed5 and COG (discussed below) only reduced membrane association of Coy1ΔTM by 15% at most, whereas the full CBD truncation diminished membrane association to nearly background levels (Figs. 4, *C* and *D*, and 6, *H* and *I*). Uncovering the interaction landscape of the CBD should improve our understanding of the contribution of Coy1 to Golgi homeostasis.

The CBD is functionally essential, as *COY1* constructs in which the highly-conserved ^{536}YERIRY^{541} or ^{604}KX_5K*XX*R^{613} sequences were mutagenized to a series of alanine residues both failed to induce a growth defect in *gos1*Δ and only partially rescued the CPY and Gas1 glycosylation defects in *coy1*Δ *sgm1*Δ (Fig. 6, *A–C*). The KX_5K*XX*R mutation also weakened the interactions between Coy1ΔTM and both Sed5 and the COG complex, indicating the first correlation between Coy1's *in vivo* function and its engagement of these interaction partners. The YERIRY mutation only modestly affected binding to Sed5 and had no effect on binding of the COG complex (Fig. 6, *D–G*), but it also modestly destabilized Coy1ΔTM's membrane association (Fig. 6, *H* and *I*), suggesting that this mutation disrupts interactions between Coy1 and factors that have yet to be identified. Neither of these mutations affected oligomerization of Coy1 (Fig. S3), suggesting that any interactions disrupted by these mutations are transient rather than stable, a conclusion supported by the observation that Coy1 and Cog3 are well-resolved from one another on both sucrose gradients (Fig. 1*A*) and by gel filtration (24). Understanding how these motifs affect

Coy1's engagement of Sed5 and the COG complex will require structural approaches.

The capability of the CBD to bind both Sed5 and the COG complex alongside its proximity to Coy1's transmembrane domain suggests a role for Coy1 in directing tethered vesicles to cognate fusion factors. Vesicle tethering is likely initiated by other golgins that act in retrograde transport, such as Rud3 or Sgm1 (7, 47–51). Once tethered, Coy1's CBD could provide a landmark that directs vesicles toward the Golgi membrane. The COG complex has been proposed to reel in tethered vesicles toward the Golgi membranes, based on the presence of N- and C-terminal COG-binding sites on the mammalian homolog of Sgm1 (52). The CBD of Coy1 not only provides a more membrane-proximal site for COG-bound vesicles, but it could also recruit Sed5 and potentially other cognate SNAREs into the vicinity of the COG-bound vesicle. It is unclear whether a single CBD can bind to COG and Sed5 simultaneously, but oligomerization of Coy1 could provide a mechanism to cluster these tethering and fusion factors together.

Higher-order assembly of Coy1 also depends on the CBD, as truncation of this region completely shifts Coy1 to the earliest fractions of the gradient. However, the GFP–CBD construct migrates at the top of the gradient, indicating that although this region is necessary for oligomerization of Coy1, it cannot form a higher-order structure on its own (Fig. 5). Notably, mutations within the CBD that disrupt the binding of Coy1 to Sed5 and COG had no detectable effect on the size of the Coy1 complex, suggesting that binding of the CBD to these proteins does not contribute substantial bulk to the size of the Coy1 complex (Fig. 6, *A–G*, and Fig. S3). The fact that this domain does not form a larger complex on its own suggests that oligomerization of Coy1 depends on coordination between the CBD and Coy1's coiled-coil domains.

Indeed, the most C-terminal coiled-coil domain is also required for Coy1 to stably assemble into a higher-order structure (Fig. 2). Mutation of conserved residues within this coiled-coil reduce oligomerization of Coy1 and disrupt its *in vivo* function, suggesting that oligomerization is essential for Coy1 to contribute to Golgi retrograde transport (Figs. 6, *A–C*, 7, *A–C*, and 8 and Fig. S3). It is unclear whether the CBD, the C-terminal coiled-coil, or both domains form the oligomerization interface. However, the finding that truncation of the CBD, but not the C-terminal coiled-coil, completely shifts Coy1 to the top of the gradient suggests that the CBD forms the primary oligomerization interface. The milder shift observed when the C-terminal coiled-coil is deleted or mutated is consistent with a role for this domain in either stabilizing or promoting assembly of this complex. Although coiled-coils typically assemble into dimers, trimers, or tetramers, larger assemblies braced by coiled-coils have recently been discovered in native and engineered proteins (53–56). These structures offer a framework for considering how the C-terminal coiled-coil may enable oligomerization of Coy1. Further studying how the C-terminal coiled-coil domain and CBD collaborate to define the oligomeric state of Coy1 will be essential to understanding its function in retrograde transport at the Golgi complex.

Our data suggest that the interactions between the CBD, COG complex, and Sed5 are influenced by Coy1's coiled-coils. A Coy1 construct lacking the coiled-coil domains binds these interaction partners more robustly than full-length Coy1, suggesting that these interactions are autoinhibited by the coiled-coil region. As this effect is only observed after truncation of the entire coiled-coil region and is not apparent when only the most N-terminal coiled-coil domains are truncated (Fig. 3, *A–D*), this restriction is likely attributable to the middle coiled-coil domains.

Unexpectedly, although Coy1 binds the COG complex and Sed5 when its N-terminal coiled-coils are truncated (Fig. 3, *A–E*), the QRDRFR*X*R, R497L, and R503L mutations all attenuate these interactions when the N terminus of Coy1 is intact (Figs. 6, *D–G*, and 7, *D–G*). As these mutations also destabilize the Coy1 complex (Fig. 8 and Fig. S3), these results suggest that oligomerization is required for Coy1 to engage with interaction partners. Oligomerization is not essential for binding *per se*, as the CBD alone does not sediment as a large particle, yet it robustly interacts with Sed5 and the COG complex. Moreover, the observation that full-length Coy1 persists as an oligomer yet only modestly interacts with Sed5 and the COG complex suggests that oligomerization alone does not enable these interactions (Figs. 1 and 3, *B–E*). Rather, we speculate that oligomerization is a prerequisite for relief of Coy1 autoinhibition. Restricting the activity of Coy1 until it has been incorporated into a larger complex could serve to prevent premature interactions between Coy1 and SNAREs like Sed5 that could interfere with trafficking between the ER and Golgi complex. This model is consistent with the observation that the Coy1(494–679) construct, which includes only the most C-terminal coiled-coil, elicits a more pronounced growth defect in *gos1*Δ cells than the 379–679 construct, which additionally includes the middle coiled-coil domains (Fig. S1).

Once assembled into a large complex, we speculate that Coy1 persists in a closed conformation until a signal, perhaps conveyed after the capture of a vesicle by another tethering factor, triggers rearrangement of the coiled-coil domains in a manner that relieves autoinhibition of Coy1. This conformational change would expose binding sites for the COG complex and Golgi retrograde SNAREs and provide a means for a captured vesicle to dock and initiate SNAREpin assembly. Mapping inter- and intra-molecular interactions between Coy1's coiled-coil domains and the CBD will be essential to better understand how these regions define the activation and binding mechanisms of Coy1.

Why would oligomerization of Coy1 into a megadalton-sized complex be essential for its interactions and *in vivo* function? Studies on exocytotic and vacuolar fusion have established a role for oligomeric SNARE-binding proteins in scaffolding the assembly of multiple SNAREpins to promote stable opening of a fusion pore (30, 57–61). Additionally, a recent report on the homotypic fusion and vacuole protein-sorting complex (HOPS) revealed that after SNAREpin assembly, HOPS drives the transition from hemifusion to fusion pore opening. This latter function can also be fulfilled by simply affixing large ligands, such as antibodies or the 850-kDa enzyme phosphofructokinase, to the SNAREpin. Molecular dynamics simulations suggested that during hemifusion, bulky SNARE-bound proteins like HOPS introduce a curvature strain between

Table 1
Yeast strains used in this study

Strains	Genotype	Ref.
CBY740 (BY4742)	*MATα his3Δ1 leu2Δ0 lys2Δ0 ura3Δ0*	83
CBY2660	*CBY740 with coy1Δ::kanMX6*	Research Genetics
CBY2674	*CBY740 with COY1::3HA-His3MX6*	24
CBY2679	*CBY740 with gos1Δ::kanMX6*	Research Genetics
CBY3484	*CBY740 with COY1 (1–613)::3HA-HIS3MX6*	24
CBY4102	*CBY740 with coy1Δ::kanMX6 sgm1Δ::hphMX6*	24
CBY4103	*CBY740 with coy1Δ::natMX6 rud3Δ::kanMX6 sgm1Δ::hphMX6*	24
CBY5544	*CBY2674 with kanMX6-pGAL::COY1 (211–679)*	This study
CBY5545	*CBY 2674 with kanMX6-pGAL::COY1 (536–679)*	This study

apposing membranes that is relieved by the opening of the fusion pore (62). It remains untested whether this finding is applicable to other organelles. Still, the precedents established by these studies offer some guidance on how to further explore whether oligomerization of Coy1 contributes to membrane fusion or SNAREpin assembly in a reconstituted system.

Experimental procedures

Growth media

Yeast cultures were grown in YP (2% bacto-peptone, 1% bacto-yeast extract (BD Biosciences)). Cultures carrying plasmids were maintained in auxotrophic selective media (0.7% yeast nitrogen base without amino acids (BD Biosciences)) with Complete Supplement Media (MP Biomedicals, Solon, OH). Unless otherwise indicated, cultures were grown in 2% glucose. To induce expression of constructs under the *GAL1* promoter, cultures were first grown overnight in 3% raffinose and then back-diluted in media with 2% galactose (Millipore Sigma).

Yeast strain construction

Transformations into yeast were performed using the lithium acetate method (63, 64). Yeast strains used in this study are listed in Table 1. The *pGAL-COY1*(211–679)-*3xHA* (CBY5544) and *pGAL-COY1*(536–679)-*3xHA* (CBY5545) strains were constructed through gene targeting (65). The *pFA6a-kanmx6-pGAL1* cassette was amplified with the primers NA203 and NA204 or NA205 and NA206, respectively, which were designed to N-terminally truncate Coy1 at the indicated residues. The fragments were transformed into *COY1–3xHA* (CBY2674). Transformants were subjected to selection on YPD with 0.5 μg/ml G418 and screened by immunoblotting (Thermo Fisher Scientific, Waltham, MA).

Plasmid construction

Plasmids used in this study are listed in Table 2, and primers are listed in Table S1 of the supporting information. The sequence of the constructs described below were verified by Sanger cycle sequencing by the Dartmouth Molecular Biology Shared Resource facility.

To construct the Coy1ΔCC plasmids, predicted coiled-coil domains were identified using Marcoil (32, 33) and deleted from the *COY1* sequence on pRS426 *COY1* (22) using the QuikChange site–directed mutagenesis kit (Stratagene, La Jolla, CA) with the modifications described by Liu and Naismith (66). Coy1ΔCC1 was constructed with primers NA046 and NA047; ΔCC2 with NA065 and NA066; ΔCC3 with NA036 and NA037; ΔCC4 with p038 and p039; ΔCC5 with NA050 and NA051; and ΔCC6 with NA052 and NA053.

Table 2
Plasmids used in this study

Strain no.r	Plasmid name	Ref.
CBB 307	pRS425	84
CBB 308	pRS426	84
CBB 3547	YIPlac204-TC-Sec7–6xDsRed-M1	67
CBB 3733	pRS426 pPHO5 Coy1	22
CBB 4067	pRS316 pTPI GFP P4M	S. Weiss[a]
CBB 4241	pSH47	68
CBB 4262	pRS426 pPHO5 Coy1ΔCC3	This study
CBB 4264	pRS426 pPHO5 Coy1ΔCC4	This study
CBB 4296	pRS426 pPHO5 Coy1ΔCC1	This study
CBB 4297	pRS426 pPHO5 Coy1ΔCC2	This study
CBB 4298	pRS426 pPHO5 Coy1ΔCC5	This study
CBB 4299	pRS426 pPHO5 Coy1ΔCC6	This study
CBB 4930	pRS425 pTPI	S. Weiss[a]
CBB 5075	pRS425 pTPI 3xHA	This study
CBB 5427	pRS416 pGAL Coy1 KX_5KX_2R	This study
CBB 5461	pRS425 pGAL Coy1 (1–613) 3xHA	This study
CBB 5462	pRS425 pGAL Coy1 (1–535) 3xHA	This study
CBB 5473	pRS416 pGAL Coy1 QRDRFRXR	This study
CBB 5474	pRS416 pGAL Coy1 YERIRY	This study
CBB 5475	pFA6a-link-GFPEnvy-SpHis5	35
CBB 5522	pRS425 pTPI GFPEnvy 3xHA	This study
CBB 5524	pRS425 pTPI GFPEnvy Coy1 (536–613) 3xHA	This study
CBB 5569	pRS316 pTPI Coy1 3xHA	This study
CBB 5570	pRS316 pTPI Coy1 3xHA QRDRFRxR	This study
CBB 5571	pRS316 pTPI Coy1 3xHA YERIRY	This study
CBB 5572	pRS316 pTPI Coy1 3xHA KX_5KX_2R	This study
CBB 5573	pRS316 pTPI Coy1 (1–613) 3xHA	This study
CBB 5574	pRS316 pTPI Coy1 (1–613) 3xHA QRDRFRXR	This study
CBB 5575	pRS316 pTPI Coy1 (1–613) 3xHA YERIRY	This study
CBB 5576	pRS316 pTPI Coy1 (1–613) 3xHA KX_5KX_2R	This study
CBB 5577	pRS316 pTPI Coy1 (1–535) 3xHA	This study
CBB 5581	pRS416 pGAL Coy1 3xHA	This study
CBB 5582	pRS416 pGAL Coy1 (233–679) 3xHA	This study
CBB 5583	pRS416 pGAL Coy1 (379–679) 3xHA	This study
CBB 5584	pRS416 pGAL Coy1 (494–679) 3xHA	This study
CBB 5585	pRS416 pGAL Coy1 (536–679) 3xHA	This study
CBB 5624	pRS416 pGAL Coy1 R497L	This study
CBB 5625	pRS416 pGAL Coy1 R503L	This study
CBB 5628	pRS416 pGAL Coy1 F500L	This study
CBB 5629	pRS316 pTPI Coy1–3xHA R497L	This study
CBB 5643	pRS316 pTPI Coy1–3xHA R503L	This study
CBB 5626	pRS316 pTPI Coy1 (1–613) 3xHA R497L	This study
CBB 5627	pRS316 pTPI Coy1 (1–613) 3xHA R503L	This study

[a] S. Weiss, unpublished observations.

The pRS425 *pTPI* plasmid was built by amplifying the *TPI* promoter from *YIPlac204-TC-Sec7–6xDsRed-M1* (67) (Addgene 25448) using SWP37 and SWP38. This sequence was inserted into pRS425 through SacII and XmaI sites. The sequence encoding the 3xHA epitope and *ADH1* terminator were subsequently amplified from *pFA6a-3xHA-His3MX6* with NA178 and NA179 (65). This fragment was ligated into pRS425 *pTPI* through XhoI/ApaI sites, generating pRS425 pTPI-3xHA.

The pRS425 *pGAL COY1*(1–613)-*3xHA* and pRS425 *pGAL COY1*(1–535)-*3xHA* plasmids were constructed by amplifying

the promoter and indicated regions of *COY1* from pRS416 *pGAL COY1* using NA231 and either NA233 or NA234, respectively. Fragments were inserted into pRS425 *pTPI 3xHA* through SacI/XhoI sites.

To construct pRS416 *pGAL COY1*, *COY1* was amplified from pRS426 *COY1* with NA215 and NA218 (22). The fragment was then inserted into the pSH47 backbone through XbaI/XhoI overhangs (68).

The pRS425 *pTPI-COY1–3xHA* constructs encoding residues 1–679 or 1–535 were built by amplifying the indicated regions from pRS416 *pGAL COY1* with NA245 and either NA232 or NA234, whereas the region encoding residues 1–613 was amplified from pRS426 *pPHO5 COY1* with NA164 and NA177. The fragments were subsequently ligated into pRS425 *pTPI-3xHA* through XmaI and XhoI sites. The pRS425 *pTPI-GFP-3xHA* construct was built by amplifying the *GFPEnvy* ORF from *pFA6a-link-GFPEnvy-SpHis5* (35) (Addgene 60782) with NA244 and NA256 and then inserting this fragment into pRS425 *pTPI-xHA* through XmaI and SalI sites. The pRS425 *pTPI-GFP-CBD-3xHA* plasmid was constructed by amplifying the region encoding residues *536–613-3xHA* from pRS425 *pGAL COY1*(*1–613*)*-3xHA* with NA179 and NA248 and then ligating this fragment into pRS425 *pTPI-GFP-3xHA*.

COY1 plasmids with point mutations were constructed using the megaprimer method with modifications (69, 70). Megaprimers with the QRDRFR*X*R, YERIRY, KX_5K*XX*R, R497L, F500L, and R503L mutations were amplified with NA218 and the mutagenic primers NA240, NA241, NA239, NA269, NA268, and NA270. Megaprimers were gel-purified and used with NA215 to amplify the full *COY1* ORF. The fragments were then inserted into the pSH47 backbone through XbaI/XhoI overhangs, generating pRS416 pGAL *COY1* plasmids bearing the indicated point mutations. The *COY1* sequence was then amplified from these plasmids with NA245 and NA232 and ligated into pRS316 *pTPI-COY1*(1–613)*-3xHA*, generating the pRS316 *pTPI COY1–3xHA* mutant plasmids. The pRS416 plasmids were also used as templates to amplify *pGAL-COY1*(1–613) using NA242 and NA245 for the QRDRFR*X*R and YERIRY constructs and NA250 and NA251 for the KX_5K*XX*R construct. These fragments were then ligated into pRS425 *pTPI 3xHA* through SacI and XhoI sites, yielding the pRS425 *pGAL COY1*(1–613) 3xHA plasmids with the indicated point mutations. This *COY1*(*1–613*)*-3xHA* sequence was subsequently amplified from this pRS425 series using p242 and p245 and ligated into pRS316 pTPI through XmaI and KpnI sites, yielding pRS316 *pTPI COY1*(*1–613*)*-3xHA* point mutant constructs.

Plasmids expressing N-terminal truncations of Coy1 were constructed by amplifying the *COY1–3HA* sequence from pRS425 *pGAL-COY1–3xHA*. NA242 and either NA215(1–679), NA258(233–679), NA259(379–679), NA261(494–679), or NA224(536–679) were used as primers. The constructs were ligated into pSH47 through XbaI and KpnI sites.

Membrane preparation and yeast cell lysis

Yeast semi-intact cells were prepared as described previously (71). To prepare yeast whole-cell lysates from small scale cultures, 1 OD_{600} unit of mid-log phase yeast cells were pelleted at 4,000 rpm in an Eppendorf 5424 centrifuge for 5 min. Pellets were resuspended in 200 μl of JR lysis buffer (25 mM HEPES, pH 7.0, 50 mM KOAc, 2 mM EDTA, 1.8 mM DTT, 1.8 mM PMSF) and diluted with an equivalent volume of 5× SDS-PAGE sample buffer (125 mM Tris, pH 6.8, 30% glycerol, 4% SDS, 0.01% bromphenol blue). 100 μl of acid-washed beads were added to the samples, which were then lysed in a Mini-Beadbeater-16 (Biospec, Bartlesville, OK). Lysates were centrifuged at 14,000 × rpm in an Eppendorf 5424 centrifuge for 10 min, and the supernatant was recovered, boiled at 95 °C for 5 min, and resolved on SDS-polyacrylamide gels. Lysates from 1-liter cultures were prepared by liquid nitrogen lysis as described previously (24).

Antibodies and immunoblotting

Polyclonal antibodies against Cog2 and Cog3 (72), the COPI complex (73), Coy1 (24), GST–Yet3 (37), Erv46 (74), Sec13 (75), Sec19 (76), and Vam3 (77) have all been previously reported. Monoclonal anti-HA (HA.11) antibodies were purchased from BioLegend (San Diego, CA). All primary antibodies were diluted 1:1000 except for GST–Yet3 and Cog2 antibodies, which were used at 1:5000. Secondary donkey anti-rabbit and sheep anti-mouse antibodies were purchased from GE Healthcare and used at a 1:10,000 concentration. Immunoblot signals were developed with Supersignal West Pico chemiluminescent substrate (Thermo Fisher Scientific), detected with a G:BOX Chemi XR5, and quantified with Syngene GeneTools densitometric analysis software (Syngene, Frederick, MD). Sucrose gradient distributions were plotted with Microsoft Excel (Microsoft, Redmond, WA). All other graphs and all statistical analyses were conducted with Graphpad Prism (Graphpad Software, San Diego, CA).

Membrane and protein fractionation

Membrane association assays were conducted as described previously with modifications (24). In brief, *coy1*Δ cells expressing the indicated constructs under the constitutive *TPI* promoter on 2-μm or centromeric plasmids (in Figs. 4 and 5, respectively) were grown in selective media overnight and diluted to 0.1 OD_{600}/ml in 50 ml of YPD. Cells were harvested in mid-log phase and converted to semi-intact cells. 0.1-ml aliquots were prepared from the semi-intact cells and frozen in liquid nitrogen. Cells were subsequently resuspended in 1 ml of B88 (150 mM KOAc, 20 mM HEPES, pH 7.0, 5 mM MgOAc, 250 mM sorbitol) + 1 mM PMSF and centrifuged at 54,000 rpm in a TLA 100.3 rotor for 20 min at 4 °C. Samples of the supernatant were diluted 1:1 in 5× SDS-PAGE sample buffer, and the remaining supernatant was aspirated off. After resuspending the membrane pellet in 1.1 ml of B88, samples of the pellet were diluted in sample buffer. Supernatant and pellet fractions were then resolved on 11% SDS-polyacrylamide gels and analyzed by immunoblotting with antiserum directed against either Coy1, the HA epitope, Sec19, or Erv46.

Fractionation of proteins on sucrose gradients was conducted as described previously with modifications (73, 77–79). 5–45% continuous sucrose gradients with 25 mM HEPES, pH 8.0, 150 mM KOAc, and 1% Triton X-100 were prepared in 14 × 89-mm Ultra-Clear tubes (Beckman Coulter). 25 OD_{600} units of

the indicated yeast strains were converted to semi-intact cells and resuspended in 0.75 ml of buffer (25 mM HEPES, pH 8.0, 150 mM KOAc, 5 mM EDTA, 1 mM PMSF, 1 mM DTT) and then diluted with an equivalent volume of the same buffer supplemented with 2% Triton X-100. Samples were vortexed and incubated on ice for 15 min and then centrifuged at 54,000 rpm in a TLA 100.3 rotor for 20 min at 4 °C. 0.5 ml of the supernatant was layered on top of the gradient, and samples were centrifuged at 220,000 × *g* for 12 h at 4 °C in an SW41 rotor. 0.8-ml fractions were collected from the top to the bottom of the gradient, and fractions were diluted 1:1 in SDS-PAGE sample buffer and boiled. Samples were then resolved on 11% SDS-polyacrylamide gels and analyzed by immunoblotting with antiserum against Cop1, Coy1, Sec13, Cog3, Erv46, and Vam3. Fractionation of organelles over sucrose gradients was performed as described previously (24, 80).

Protein purification and in vitro binding assays

Recombinant proteins were purified from *Escherichia coli* as described previously (5, 24, 34, 81, 82). Binding assays were set up as described with modifications (24). 15 μl of Ni-NTA or GSH-agarose resin per reaction was washed with 1 ml of binding buffer (25 mM HEPES, pH 7.4, 150 mM KOAc, 10 mM β-mercaptoethanol, 250 mM sorbitol, 0.1% Triton X-100, and, for the Ni-NTA reactions, 30 mM imidazole) three times and incubated with 50 μg of purified protein per reaction for 1 h at room temperature with nutation and then washed three times with 1 ml of binding buffer again. The immobilized proteins were set aside while cell extract or cytosol was prepared.

For binding assays using Coy1 with an intact transmembrane domain (Fig. 3, *B–E*), 50-ml cultures of *pGAL-COY1–3xHA* (CBY2674), *pGAL-COY1*(*211–679*) (CBY5544), and *pGAL-COY1*(*536–679*) (CBY5545) were grown to mid-log in YPD at 30 °C and then diluted to 0.1 OD_{600}/ml in 1 liter of YP + 2% galactose. Growth was continued for 16 h at 30 °C, and cells were subsequently harvested by centrifugation, lysed in a blender with liquid nitrogen, and divided into aliquots corresponding to 50 mg wet weight. Cells were later resuspended in buffer (0.5 ml of 25 mM HEPES, pH 7.4, 150 mM KOAc, 10 mM β-mercaptoethanol, 250 mM sorbitol, 1 mM PMSF and, for the COG binding assays, 30 mM imidazole) and then diluted with an equivalent volume of buffer supplemented with 2% Triton X-100. Cells were briefly vortexed, incubated on ice for 15 min, and centrifuged at 54,000 rpm in a TLA 100.3 rotor for 20 min at 4 °C. 0.5 ml of the solubilized extract was then incubated with the immobilized proteins for 3 h at 4 °C, washed with 1 ml of binding buffer, and eluted by boiling in 5× sample buffer. The eluate was subsequently resolved on 11.5% gels and analyzed by immunoblotting with monoclonal antiserum against HA to monitor recovery of Coy1 and polyclonal antibodies against GST and Cog2.

For all other binding assays, *coy1*Δ cells carrying 2-μm plasmids encoding the *COY1*Δ*TM* constructs expressed under the *GAL1* promoter were grown overnight in selective media with 3% raffinose as the sole carbon source. Cells were then back-diluted to 0.1 OD_{600}/ml in 50 ml of YP + 2% galactose, grown to mid-log, and converted to semi-intact cells. Semi-intact cells were resuspended in 0.5 ml of binding buffer and snap-frozen in liquid nitrogen in 25-μl aliquots. Aliquots were resuspended in 1.1 ml of binding buffer + 1 mM PMSF and centrifuged at 54,000 rpm in a TLA 100.3 rotor for 20 min at 4 °C. 0.5 ml of the supernatant was incubated with the immobilized proteins, washed, eluted, and analyzed as described above.

Author contributions—N. S. A. data curation; N. S. A. formal analysis; N. S. A. writing-original draft; N. S. A. and C. B. writing-review and editing; C. B. supervision; C. B. funding acquisition; C. B. project administration.

Acknowledgments—We thank Amy Gladfelter, James Moseley, Bing He, and members of the Barlowe laboratory for advice and suggestions on this work and Anne Spang for providing the pSH47 plasmid.

References

1. Glick, B. S., and Luini, A. (2011) Models for Golgi traffic: a critical assessment. *Cold Spring Harb. Perspect. Biol.* **3,** a005215 CrossRef Medline
2. Fisher, P., and Ungar, D. (2016) Bridging the gap between glycosylation and vesicle traffic. *Front. Cell Dev. Biol.* **4,** 15 CrossRef Medline
3. Mizuno-Yamasaki, E., Rivera-Molina, F., and Novick, P. (2012) GTPase networks in membrane traffic. *Annu. Rev. Biochem.* **81,** 637–659 CrossRef Medline
4. Yu, I. M., and Hughson, F. M. (2010) Tethering factors as organizers of intracellular vesicular traffic. *Annu. Rev. Cell Dev. Biol.* **26,** 137–156 CrossRef Medline
5. Parlati, F., McNew, J. A., Fukuda, R., Miller, R., Söllner, T. H., and Rothman, J. E. (2000) Topological restriction of SNARE-dependent membrane fusion. *Nature* **407,** 194–198 CrossRef Medline
6. Parlati, F., Varlamov, O., Paz, K., McNew, J. A., Hurtado, D., Söllner, T. H., and Rothman, J. E. (2002) Distinct SNARE complexes mediating membrane fusion in Golgi transport based on combinatorial specificity. *Proc. Natl. Acad. Sci. U.S.A.* **99,** 5424–5429 CrossRef Medline
7. Wong, M., and Munro, S. (2014) Membrane trafficking. The specificity of vesicle traffic to the Golgi is encoded in the golgin coiled-coil proteins. *Science* **346,** 1256898 CrossRef Medline
8. Magdeleine, M., Gautier, R., Gounon, P., Barelli, H., Vanni, S., and Antonny, B. (2016) A filter at the entrance of the Golgi that selects vesicles according to size and bulk lipid composition. *Elife* **5,** e16988 CrossRef Medline
9. Yuan, H., Davis, S., Ferro-Novick, S., and Novick, P. (2017) Rewiring a Rab regulatory network reveals a possible inhibitory role for the vesicle tether, Uso1. *Proc. Natl. Acad. Sci. U.S.A.* **114,** E8637–E8645 CrossRef Medline
10. Gillingham, A. K. (2018) At the ends of their tethers! How coiled-coil proteins capture vesicles at the Golgi. *Biochem. Soc. Trans.* **46,** 43–50 CrossRef Medline
11. Malsam, J., and Söllner, T. H. (2011) Organization of SNAREs within the Golgi stack. *Cold Spring Harb. Perspect. Biol.* **3,** a005249 CrossRef Medline
12. Siniossoglou, S., and Pelham, H. R. (2001) An effector of Ypt6p binds the SNARE Tlg1p and mediates selective fusion of vesicles with late Golgi membranes. *EMBO J.* **20,** 5991–5998 CrossRef Medline
13. Suvorova, E. S., Duden, R., and Lupashin, V. V. (2002) The Sec34/Sec35p complex, a Ypt1p effector required for retrograde intra-Golgi trafficking, interacts with Golgi SNAREs and COPI vesicle coat proteins. *J. Cell Biol.* **157,** 631–643 CrossRef Medline
14. Willett, R., Kudlyk, T., Pokrovskaya, I., Schönherr, R., Ungar, D., Duden, R., and Lupashin, V. (2013) COG complexes form spatial landmarks for distinct SNARE complexes. *Nat. Commun.* **4,** 1553 CrossRef Medline
15. Dubuke, M. L., and Munson, M. (2016) The secret life of tethers: the role of tethering factors in SNARE complex regulation. *Front. Cell Dev. Biol.* **4,** 42 CrossRef Medline
16. Gillingham, A. K., and Munro, S. (2016) Finding the Golgi: golgin coiled-coil proteins show the way. *Trends Cell Biol.* **26,** 399–408 CrossRef Medline

17. Wong, M., Gillingham, A. K., and Munro, S. (2017) The golgin coiled-coil proteins capture different types of transport carriers via distinct N-terminal motifs. *BMC Biol.* **15,** 3 CrossRef Medline
18. Shin, J. J. H., Gillingham, A. K., Begum, F., Chadwick, J., and Munro, S. (2017) TBC1D23 is a bridging factor for endosomal vesicle capture by golgins at the trans-Golgi. *Nat. Cell Biol.* **19,** 1424–1432 CrossRef Medline
19. Sinka, R., Gillingham, A. K., Kondylis, V., and Munro, S. (2008) Golgi coiled-coil proteins contain multiple binding sites for Rab family G proteins. *J. Cell Biol.* **183,** 607–615 CrossRef Medline
20. Munro, S. (2011) The golgin coiled-coil proteins of the Golgi apparatus. *Cold Spring Harb. Perspect. Biol.* **3,** a005256 CrossRef Medline
21. Cheung, P. Y., Limouse, C., Mabuchi, H., and Pfeffer, S. R. (2015) Protein flexibility is required for vesicle tethering at the Golgi. *Elife* **4,** e12790 CrossRef Medline
22. Gillingham, A. K., Pfeifer, A. C., and Munro, S. (2002) CASP, the alternatively spliced product of the gene encoding the CCAAT-displacement protein transcription factor, is a Golgi membrane protein related to giantin. *Mol. Biol. Cell* **13,** 3761–3774 CrossRef Medline
23. Malsam, J., Satoh, A., Pelletier, L., and Warren, G. (2005) Golgin tethers define subpopulations of COPI vesicles. *Science* **307,** 1095–1098 CrossRef Medline
24. Anderson, N. S., Mukherjee, I., Bentivoglio, C. M., and Barlowe, C. (2017) The golgin protein Coy1 functions in intra-Golgi retrograde transport and interacts with the COG complex and Golgi SNAREs. *Mol. Biol. Cell* **28,** 2686–2700 CrossRef Medline
25. Waters, M. G., Clary, D. O., and Rothman, J. E. (1992) A novel 115-kD peripheral membrane protein is required for intercisternal transport in the Golgi stack. *J. Cell Biol.* **118,** 1015–1026 CrossRef Medline
26. Waters, M. G., Serafini, T., and Rothman, J. E. (1991) Coatomer: a cytosolic protein complex containing subunits of non-clathrin-coated Golgi transport vesicles. *Nature* **349,** 248–251 CrossRef Medline
27. Duden, R., Kajikawa, L., Wuestehube, L., and Schekman, R. (1998) ϵ-COP is a structural component of coatomer that functions to stabilize α-COP. *EMBO J.* **17,** 985–995 CrossRef Medline
28. Lederkremer, G. Z., Cheng, Y., Petre, B. M., Vogan, E., Springer, S., Schekman, R., Walz, T., and Kirchhausen, T. (2001) Structure of the Sec23p/24p and Sec13p/31p complexes of COPII. *Proc. Natl. Acad. Sci. U.S.A.* **98,** 10704–10709 CrossRef Medline
29. Welsh, L. M., Tong, A. H., Boone, C., Jensen, O. N., and Otte, S. (2006) Genetic and molecular interactions of the Erv41p–Erv46p complex involved in transport between the endoplasmic reticulum and Golgi complex. *J. Cell Sci.* **119,** 4730–4740 CrossRef Medline
30. Price, A., Seals, D., Wickner, W., and Ungermann, C. (2000) The docking stage of yeast vacuole fusion requires the transfer of proteins from a cis-SNARE complex to a Rab/Ypt protein. *J. Cell Biol.* **148,** 1231–1238 CrossRef Medline
31. Weill, U., Arakel, E. C., Goldmann, O., Golan, M., Chuartzman, S., Munro, S., Schwappach, B., and Schuldiner, M. (2018) Toolbox: creating a systematic database of secretory pathway proteins uncovers new cargo for COPI. *Traffic* **19,** 370–379 CrossRef Medline
32. Delorenzi, M., and Speed, T. (2002) An HMM model for coiled-coil domains and a comparison with PSSM-based predictions. *Bioinformatics* **18,** 617–625 CrossRef Medline
33. Zimmermann, L., Stephens, A., Nam, S. Z., Rau, D., Kübler, J., Lozajic, M., Gabler, F., Söding, J., Lupas, A. N., and Alva, V. (2018) A completely reimplemented MPI bioinformatics toolkit with a new HHpred server at its core. *J. Mol. Biol.* **430,** 2237–2243 CrossRef Medline
34. Lees, J. A., Yip, C. K., Walz, T., and Hughson, F. M. (2010) Molecular organization of the COG vesicle tethering complex. *Nat. Struct. Mol. Biol.* **17,** 1292–1297 CrossRef Medline
35. Slubowski, C. J., Funk, A. D., Roesner, J. M., Paulissen, S. M., and Huang, L. S. (2015) Plasmids for C-terminal tagging in *Saccharomyces cerevisiae* that contain improved GFP proteins, Envy and Ivy. *Yeast* **32,** 379–387 CrossRef Medline
36. Garrett, M. D., Zahner, J. E., Cheney, C. M., and Novick, P. J. (1994) GDI1 encodes a GDP dissociation inhibitor that plays an essential role in the yeast secretory pathway. *EMBO J.* **13,** 1718–1728 CrossRef Medline
37. Wilson, J. D., and Barlowe, C. (2010) Yet1p and Yet3p, the yeast homologs of BAP29 and BAP31, interact with the endoplasmic reticulum translocation apparatus and are required for inositol prototrophy. *J. Biol. Chem.* **285,** 18252–18261 CrossRef Medline
38. Finn, R. D., Coggill, P., Eberhardt, R. Y., Eddy, S. R., Mistry, J., Mitchell, A. L., Potter, S. C., Punta, M., Qureshi, M., Sangrador-Vegas, A., Salazar, G. A., Tate, J., and Bateman, A. (2016) The Pfam protein families database: towards a more sustainable future. *Nucleic Acids Res.* **44,** D279–D285 CrossRef Medline
39. Waterhouse, A. M., Procter, J. B., Martin, D. M., Clamp, M., and Barton, G. J. (2009) Jalview Version 2–a multiple sequence alignment editor and analysis workbench. *Bioinformatics* **25,** 1189–1191 CrossRef Medline
40. Harbury, P. B., Zhang, T., Kim, P. S., and Alber, T. (1993) A switch between two-, three-, and four-stranded coiled-coils in GCN4 leucine zipper mutants. *Science* **262,** 1401–1407 CrossRef Medline
41. Lupas, A. N., and Bassler, J. (2017) Coiled-coils–a model system for the 21st century. *Trends Biochem. Sci.* **42,** 130–140 CrossRef Medline
42. Simm, D., Hatje, K., and Kollmar, M. (2015) Waggawagga: comparative visualization of coiled-coil predictions and detection of stable single α-helices (SAH domains). *Bioinformatics* **31,** 767–769 CrossRef Medline
43. Grigoryan, G., and Keating, A. E. (2008) Structural specificity in coiled-coil interactions. *Curr. Opin. Struct. Biol.* **18,** 477–483 CrossRef Medline
44. Burgess, N. K., Stanley, A. M., and Fleming, K. G. (2008) Determination of membrane protein molecular weights and association equilibrium constants using sedimentation equilibrium and sedimentation velocity. *Methods Cell Biol.* **84,** 181–211 CrossRef Medline
45. Hopper, J. T., Yu, Y. T., Li, D., Raymond, A., Bostock, M., Liko, I., Mikhailov, V., Laganowsky, A., Benesch, J. L., Caffrey, M., Nietlispach, D., and Robinson, C. V. (2013) Detergent-free mass spectrometry of membrane protein complexes. *Nat Methods* **10,** 1206–1208 CrossRef Medline
46. Gupta, K., Donlan, J. A. C., Hopper, J. T. S., Uzdavinys, P., Landreh, M., Struwe, W. B., Drew, D., Baldwin, A. J., Stansfeld, P. J., and Robinson, C. V. (2017) The role of interfacial lipids in stabilizing membrane protein oligomers. *Nature* **541,** 421–424 CrossRef Medline
47. Kim, D. W., Sacher, M., Scarpa, A., Quinn, A. M., and Ferro-Novick, S. (1999) High-copy suppressor analysis reveals a physical interaction between Sec34p and Sec35p, a protein implicated in vesicle docking. *Mol. Biol. Cell* **10,** 3317–3329 CrossRef Medline
48. Kim, D. W. (2003) Characterization of Grp1p, a novel cis-Golgi matrix protein. *Biochem. Biophys. Res. Commun.* **303,** 370–378 CrossRef Medline
49. VanRheenen, S. M., Cao, X., Sapperstein, S. K., Chiang, E. C., Lupashin, V. V., Barlowe, C., and Waters, M. G. (1999) Sec34p, a protein required for vesicle tethering to the yeast Golgi apparatus, is in a complex with Sec35p. *J. Cell Biol.* **147,** 729–742 CrossRef Medline
50. Fridmann-Sirkis, Y., Siniossoglou, S., and Pelham, H. R. (2004) TMF is a golgin that binds Rab6 and influences Golgi morphology. *BMC Cell Biol.* **5,** 18 CrossRef Medline
51. Siniossoglou, S. (2005) Affinity purification of Ypt6 effectors and identification of TMF/ARA160 as a Rab6 interactor. *Methods Enzymol.* **403,** 599–607 CrossRef Medline
52. Miller, V. J., Sharma, P., Kudlyk, T. A., Frost, L., Rofe, A. P., Watson, I. J., Duden, R., Lowe, M., Lupashin, V. V., and Ungar, D. (2013) Molecular insights into vesicle tethering at the Golgi by the conserved oligomeric Golgi (COG) complex and the golgin TATA element modulatory factor (TMF). *J. Biol. Chem.* **288,** 4229–4240 CrossRef Medline
53. Koronakis, V., Sharff, A., Koronakis, E., Luisi, B., and Hughes, C. (2000) Crystal structure of the bacterial membrane protein TolC central to multidrug efflux and protein export. *Nature* **405,** 914–919 CrossRef Medline
54. Dong, C., Beis, K., Nesper, J., Brunkan-Lamontagne, A. L., Clarke, B. R., Whitfield, C., and Naismith, J. H. (2006) Wza the translocon for E. coli capsular polysaccharides defines a new class of membrane protein. *Nature* **444,** 226–229 CrossRef Medline
55. Liu, J., Zheng, Q., Deng, Y., Cheng, C. S., Kallenbach, N. R., and Lu, M. (2006) A seven-helix coiled-coil. *Proc. Natl. Acad. Sci. U.S.A.* **103,** 15457–15462 CrossRef Medline
56. Sun, L., Young, L. N., Zhang, X., Boudko, S. P., Fokine, A., Zbornik, E., Roznowski, A. P., Molineux, I. J., Rossmann, M. G., and Fane, B. A. (2014)

Icosahedral bacteriophage ϕX174 forms a tail for DNA transport during infection. *Nature* **505,** 432–435 CrossRef Medline
57. Shi, L., Shen, Q. T., Kiel, A., Wang, J., Wang, H. W., Melia, T. J., Rothman, J. E., and Pincet, F. (2012) SNARE proteins: one to fuse and three to keep the nascent fusion pore open. *Science* **335,** 1355–1359 CrossRef Medline
58. Wang, J., Bello, O., Auclair, S. M., Wang, J., Coleman, J., Pincet, F., Krishnakumar, S. S., Sindelar, C. V., and Rothman, J. E. (2014) Calcium sensitive ring-like oligomers formed by synaptotagmin. *Proc. Natl. Acad. Sci. U.S.A.* **111,** 13966–13971 CrossRef Medline
59. Wang, J., Li, F., Bello, O. D., Sindelar, C. V., Pincet, F., Krishnakumar, S. S., and Rothman, J. E. (2017) Circular oligomerization is an intrinsic property of synaptotagmin. *Elife* **6,** e27441 CrossRef Medline
60. Orr, A., Song, H., Rusin, S. F., Kettenbach, A. N., and Wickner, W. (2017) HOPS catalyzes the interdependent assembly of each vacuolar SNARE into a SNARE complex. *Mol. Biol. Cell* **28,** 975–983 CrossRef Medline
61. Bello, O. D., Jouannot, O., Chaudhuri, A., Stroeva, E., Coleman, J., Volynski, K. E., Rothman, J. E., and Krishnakumar, S. S. (2018) Synaptotagmin oligomerization is essential for calcium control of regulated exocytosis. *Proc. Natl. Acad. Sci. U.S.A.* **115,** E7624–E7631 CrossRef Medline
62. D'Agostino, M., Risselada, H. J., Lürick, A., Ungermann, C., and Mayer, A. (2017) A tethering complex drives the terminal stage of SNARE-dependent membrane fusion. *Nature* **551,** 634–638 CrossRef Medline
63. Ito, H., Fukuda, Y., Murata, K., and Kimura, A. (1983) Transformation of intact yeast cells treated with alkali cations. *J. Bacteriol.* **153,** 163–168 Medline
64. Gietz, R. D., and Schiestl, R. H. (2007) Quick and easy yeast transformation using the LiAc/SS carrier DNA/PEG method. *Nat. Protoc.* **2,** 35–37 CrossRef Medline
65. Longtine, M. S., McKenzie, A., 3rd., Demarini, D. J., Shah, N. G., Wach, A., Brachat, A., Philippsen, P., and Pringle, J. R. (1998) Additional modules for versatile and economical PCR-based gene deletion and modification in *Saccharomyces cerevisiae*. *Yeast* **14,** 953–961 CrossRef Medline
66. Liu, H., and Naismith, J. H. (2008) An efficient one-step site-directed deletion, insertion, single and multiple-site plasmid mutagenesis protocol. *BMC Biotechnol.* **8,** 91 CrossRef Medline
67. Losev, E., Reinke, C. A., Jellen, J., Strongin, D. E., Bevis, B. J., and Glick, B. S. (2006) Golgi maturation visualized in living yeast. *Nature* **441,** 1002–1006 CrossRef Medline
68. Güldener, U., Heck, S., Fielder, T., Beinhauer, J., and Hegemann, J. H. (1996) A new efficient gene disruption cassette for repeated use in budding yeast. *Nucleic Acids Res.* **24,** 2519–2524 CrossRef Medline
69. Sarkar, G., and Sommer, S. S. (1990) The "megaprimer" method of site-directed mutagenesis. *BioTechniques* **8,** 404–407 Medline
70. Xu, Z., Colosimo, A., and Gruenert, D. C. (2003) Site-directed mutagenesis using the megaprimer method. *Methods Mol. Biol.* **235,** 203–207 CrossRef Medline
71. Baker, D., Hicke, L., Rexach, M., Schleyer, M., and Schekman, R. (1988) Reconstitution of SEC gene product-dependent intercompartmental protein transport. *Cell* **54,** 335–344 CrossRef Medline
72. Ballew, N., Liu, Y., and Barlowe, C. (2005) A Rab requirement is not bypassed in SLY1–20 suppression. *Mol. Biol. Cell* **16,** 1839–1849 CrossRef Medline
73. Duden, R., Hosobuchi, M., Hamamoto, S., Winey, M., Byers, B., and Schekman, R. (1994) Yeast β- and β'-coat proteins (COP). Two coatomer subunits essential for endoplasmic reticulum-to-Golgi protein traffic. *J. Biol. Chem.* **269,** 24486–24495 Medline
74. Otte, S., Belden, W. J., Heidtman, M., Liu, J., Jensen, O. N., and Barlowe, C. (2001) Erv41p and Erv46p: new components of COPII vesicles involved in transport between the ER and Golgi complex. *J. Cell Biol.* **152,** 503–518 CrossRef Medline
75. Salama, N. R., Yeung, T., and Schekman, R. W. (1993) The Sec13p complex and reconstitution of vesicle budding from the ER with purified cytosolic proteins. *EMBO J.* **12,** 4073–4082 CrossRef Medline
76. Barlowe, C. (1997) Coupled ER to Golgi transport reconstituted with purified cytosolic proteins. *J. Cell Biol.* **139,** 1097–1108 CrossRef Medline
77. Ungermann, C., Sato, K., and Wickner, W. (1998) Defining the functions of trans-SNARE pairs. *Nature* **396,** 543–548 CrossRef Medline
78. Duden, R., Griffiths, G., Frank, R., Argos, P., and Kreis, T. E. (1991) β-COP, a 110 kd protein associated with non-clathrin-coated vesicles and the Golgi complex, shows homology to β-adaptin. *Cell* **64,** 649–665 CrossRef Medline
79. Conibear, E., and Stevens, T. H. (2000) Vps52p, Vps53p, and Vps54p form a novel multisubunit complex required for protein sorting at the yeast late Golgi. *Mol. Biol. Cell* **11,** 305–323 CrossRef Medline
80. Powers, J., and Barlowe, C. (1998) Transport of axl2p depends on erv14p, an ER-vesicle protein related to the *Drosophila* cornichon gene product. *J. Cell Biol.* **142,** 1209–1222 CrossRef Medline
81. Tsui, M. M., and Banfield, D. K. (2000) Yeast Golgi SNARE interactions are promiscuous. *J. Cell Sci.* **113,** 145–152 Medline
82. Peng, R., and Gallwitz, D. (2002) Sly1 protein bound to Golgi syntaxin Sed5p allows assembly and contributes to specificity of SNARE fusion complexes. *J. Cell Biol.* **157,** 645–655 CrossRef Medline
83. Brachmann, C. B., Davies, A., Cost, G. J., Caputo, E., Li, J., Hieter, P., and Boeke, J. D. (1998) Designer deletion strains derived from *Saccharomyces cerevisiae* S288C: a useful set of strains and plasmids for PCR-mediated gene disruption and other applications. *Yeast* **30,** 115–132 CrossRef Medline
84. Christianson, T. W., Sikorski, R. S., Dante, M., Shero, J. H., and Hieter, P. (1992) Multifunctional yeast high-copy-number shuttle vectors. *Gene* **2,** 119–122 Medline